Supporting Information

A host-guest interaction activated Bobbitt oxidant for highly efficient oxidation of alcohols

Jinyang Wu,‡ Youran Luo,‡ Lingxuan Chen, Xuan Sun, Xinnan Chen, Song Qin, Wen Feng,* Xiaowei Li,* and Lihua Yuan*

Key Laboratory of Radiation Physics and Technology of Ministry of Education, Institute of Nuclear Science and Technology, College of Chemistry, Sichuan University, Chengdu 610065

‡These authors contributed equally to the work.

E-mail: lhyuan@scu.edu.cn
wfeng9510@scu.edu.cn
lixw@scu.edu.cn

Table of Contents

Materials and methods

All chemicals were obtained from commercial suppliers and were used as received unless other-wise noted. Solvents were dried and distilled following usual protocols. Solvents for NMR were purchased from Cambridge Isotope Laboratories (CIL). Analytical NMR spectra were recorded on Bruker AVANCE AV II-400/600 MHz at room temperature of 298 K (^{1}H: 400 MHz; 2D: 600 MHz). Chemical shifts are reported in δ values in ppm using tetramethylsilane (TMS) or residual solvent as internal standard and coupling constants (J) are denoted in Hz. Multiplicities are denoted as follows: s = singlet, d = doublet, t = triplet, dd = double doublet and m = multiplet. MALDI-TOF mass spectrum was recorded on a Bruker Autoflex III mass spectrometer, matrix is 2,6-dihydroxyacetophenone (DHAP). High resolution mass (HRMS) data were collected by WATERS Q-TOF Premier. UV-vis spectra were measured by SHIMADZU UV-2450. Conductivity experiments were implemented on DDSJ-308A (Shanghai Precision Instruments Co., Ltd.). Single crystal X-ray data were measured on a Xcalibur E diffractometer with graphite monochromated Cu-Kα radiation (λ=1.54184 Å). Data collection and structure refinement details can be found in the CIF files or obtained free of charge via *https://www.ccdc.cam.ac.uk/*.

Synthesis and characterization

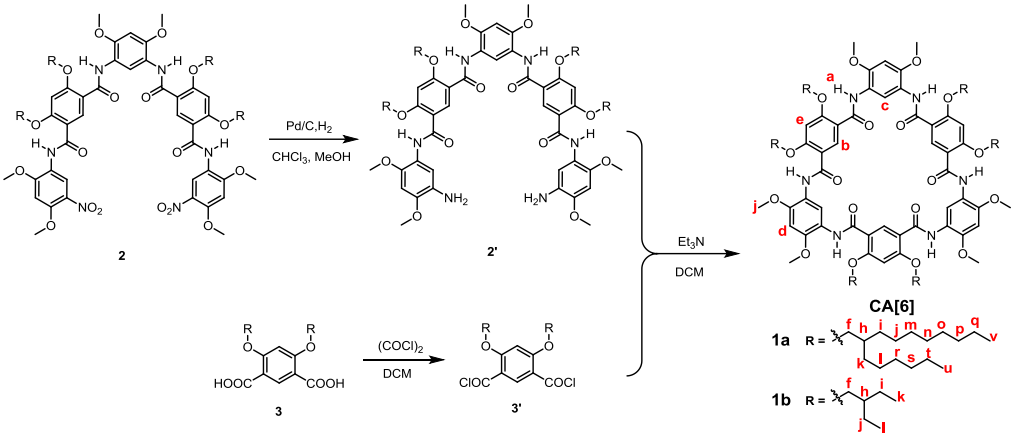

Scheme S1 Synthetic route of **1a** and **1b**.

1a and **1b** were prepared according to literature procedures. [1]

1a, white solid power (yield: 84.3 %). ^{1}H NMR (400 MHz, $CDCl_3$, 298 K) δ 9.41 (s, 3H, H_a), 9.40 (s, 3H, H_c), 9.32 (s, 6H, H_b), 6.50 (s, 3H, H_e), 6.48 (s, 3H, H_d), 4.08 (d, J = 5.8 Hz, 12H, H_f), 3.86 (s, 18H, H_j), 2.06 (p, J = 6.1 Hz, 6H, H_h), 1.52 (h, J = 7.7, 7.0 Hz, 48H, H_{i-l}), 1.43 – 1.19 (m, 128H, H_{m-t}), 0.86 (td, J = 6.8, 2.2 Hz, 36H, $H_{v/u}$). MADLI-TOF MS m/z calculated for $C_{144}H_{234}N_6O_{18}$ $[M+H]^+$ 2337.768, found 2337.422.

1b, white solid power (yield: 80.4 %). ^{1}H NMR (400 MHz, $CDCl_3$, 298 K) δ 9.73 – 9.66 (m, 3H, H_a), 9.63 – 9.55 (m, 6H, H_b), 9.20 (dd, J = 5.2, 2.4 Hz, 3H, H_c), 6.61 (t, J = 3.3 Hz, 6H, $H_{d/e}$), 4.20 (d, J = 5.0 Hz, 12H, H_f), 3.95 (dd, J = 3.8, 1.7 Hz, 18H, H_j), 2.21 (m, 6H, H_h), 1.63 (q, J = 6.8 Hz, 24H, $H_{i/j}$), 1.03 (m, J = 7.9, 2.9, 2.3 Hz, 36H, $H_{k/l}$). MADLI-TOF MS m/z calculated for $C_{84}H_{114}N_6O_{18}$ $[M+H]^+$ 1495.826, found 1495.890.

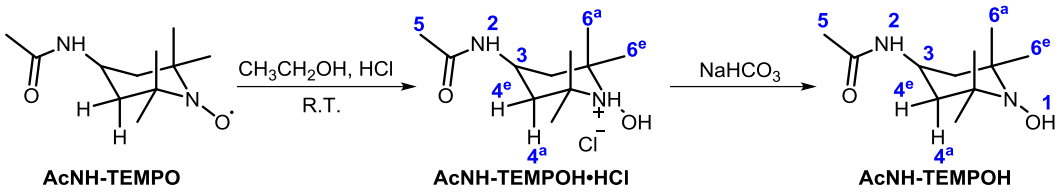

Scheme S2 Synthetic routes of **AcNH-TEMPOH**.

The compounds of **AcNH-TEMPOH·HCl** and **AcNH-TEMPOH** were prepared according to the literature procedures. [2]

AcNH-TEMPOH·HCl: white solid power (yield: 78.6 %). ^{1}H NMR (400 MHz, D_2O, 298 K) δ 4.21 (m, J = 12.5, 7.8, 3.9 Hz, 1H, H_3), 2.17 – 2.08 (m, 2H, H_4^e), 1.90 (s, 3H, H_5), 1.71 (t, J = 13.3 Hz, 2H, H_4^a), 1.42 (s, 6H, H_6^e), 1.37 (s, 6H, H_6^a).

AcNH-TEMPOH: ^{1}H NMR (400 MHz, D_2O, 298 K) δ 4.087 (m, J = 12.5, 7.8, 3.9 Hz, 1H, H_3),1.89 (s, 3H, H_5), 1.84 (m, J = 13.4, 3.4, 1.6 Hz, 2H, H_4^e), 1.43 (t, J = 12.8 Hz, 2H, H_4^a), 1.18 (s, 6H, H_6^e), 1.14 (s, 6H, H_6^a).

Host-guest chemistry of 1a and AcNH-TEMPO$^+$BF$_4^-$

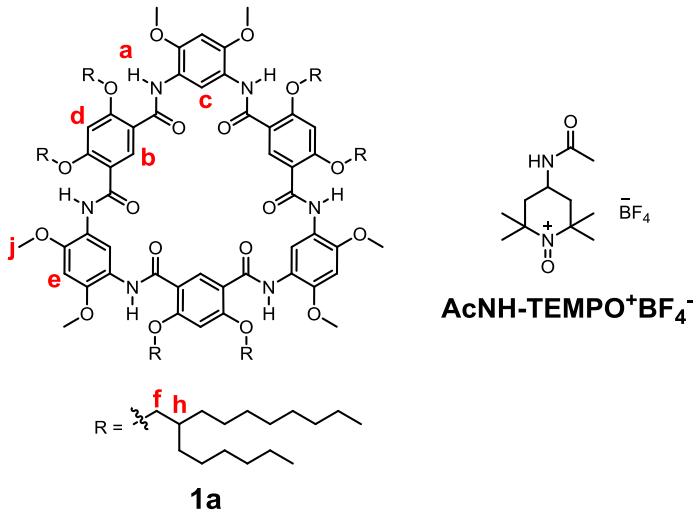

Scheme S3 Chemical structures of **1a** (host) and **AcNH-TEMPO$^+$BF$_4^-$** (guest)**.**

Guest **(AcNH-TEMPO$^+$BF$_4^-$)** was obtained from commercial supplier (Tokyo Chemical Industry, TCI) and was used as received.

Job plot for determination of stoichiometry

Because of the poor solubility of guest **AcNH-TEMPO$^+$BF$_4^-$** in $CHCl_3$, the mixed solvent of $CHCl_3/CH_3CN$ (5:1, v/v) was used for Job plot and binding constant.

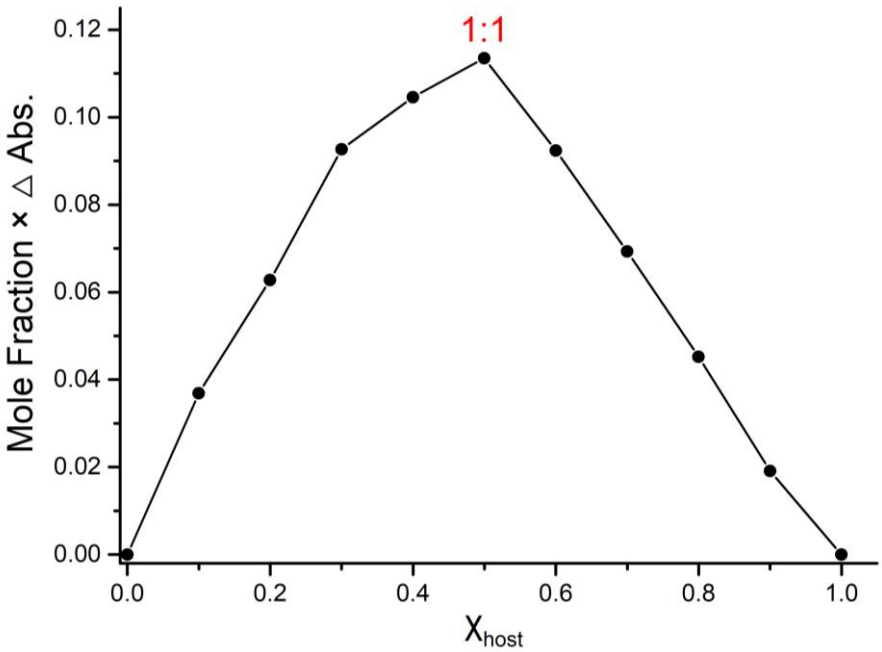

Figure S1 Job plot for determination of stoichiometry of **1a** and **AcNH-TEMPO$^+$BF$_4^-$** based on the absorbance at 365 nm in $CHCl_3/CH_3CN$ (5:1, v/v, 298 K). [**1a**] + [**AcNH-TEMPO$^+$BF$_4^-$**] = 50 μM.

HRMS spectra of AcNH-TEMPO$^+$BF$_4^-$⊂1a

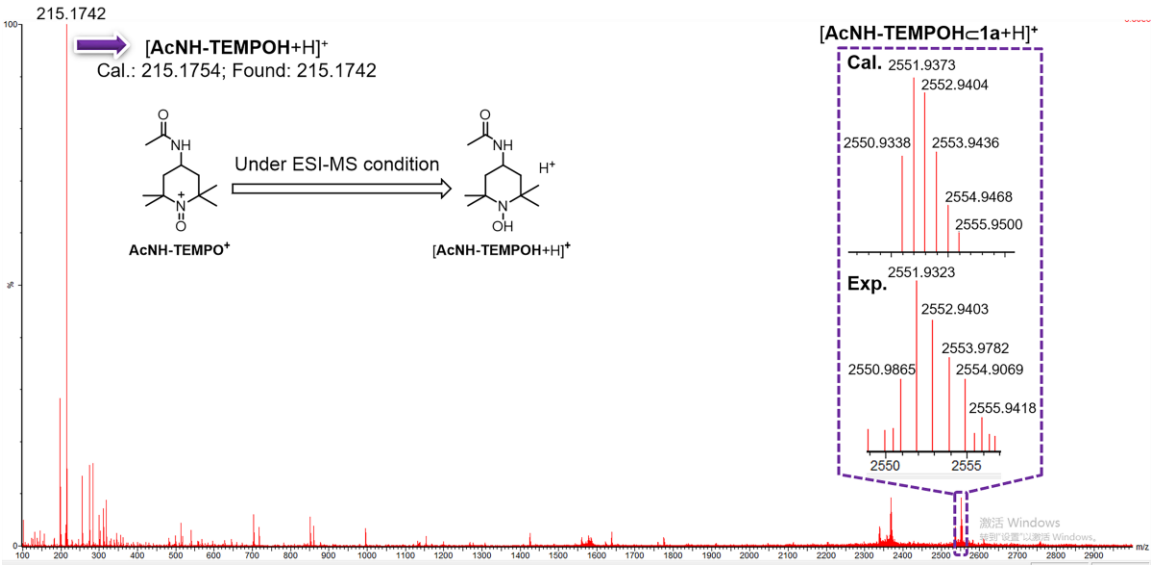

Figure S2 Full HRMS spectrum of **AcNH-TEMPOH⊂1a** complex derived from **AcNH-TEMPO$^+$BF$_4^-$⊂1a** complex in $CHCl_3/CH_3CN$ (5:1, v/v) under ESI-MS condition. The **AcNH-TEMPOH⊂1a** complex was produced in situ from a mixture of **AcNH-TEMPO$^+$BF$_4^-$** and **1a**. HRMS (ESI) calculated for [**1a**+**AcNH-TEMPOH**+H]$^+$, m/z, 2551.9373, found 2551.9323.

UV-vis titration experiments

To determinate the binding constant (K_a) of macrocycle **1a** and guest **AcNH-TEMPO$^+$BF$_4^-$**, UV-vis titration experiments were performed in $CHCl_3/CH_3CN$ (5:1, v/v, 298 K) at a constant concentration of **1a** (50 μM) and varying concentration of **AcNH-TEMPO$^+$BF$_4^-$**. For the titration, at least 20 data points were collected. Binding constant was calculated by a global fitting analysis according to a 1:1 binding model using the website *(http://supramolecular.org/)*.

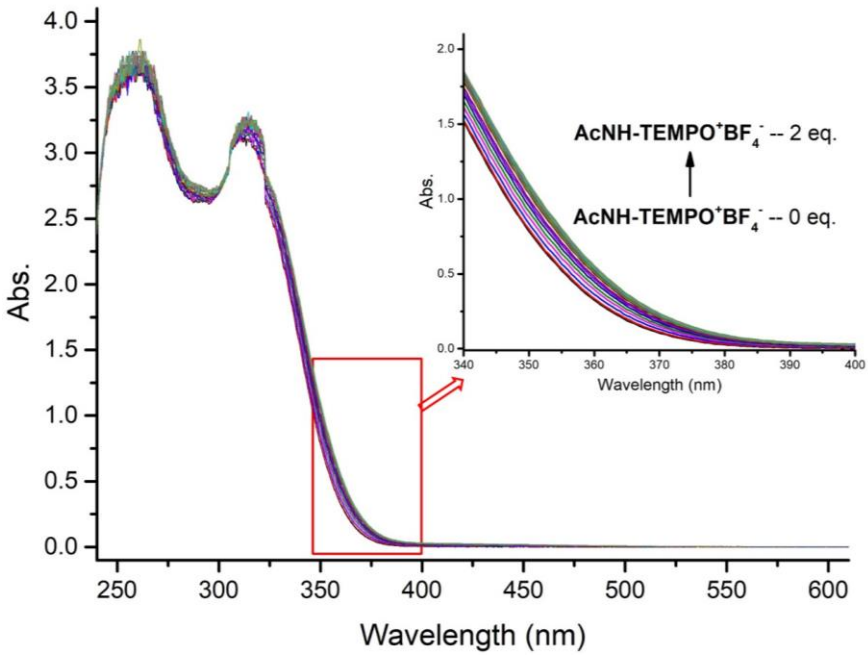

Figure S3 Stacked UV-vis spectra of **1a** (50 μM) titrated with **AcNH-TEMPO⁺BF₄⁻** in $CHCl_3/CH_3CN$ (5:1, v/v) at 298 K**.** Inserted are expanded spectra in the wavelength range from 340 nm to 400 nm.

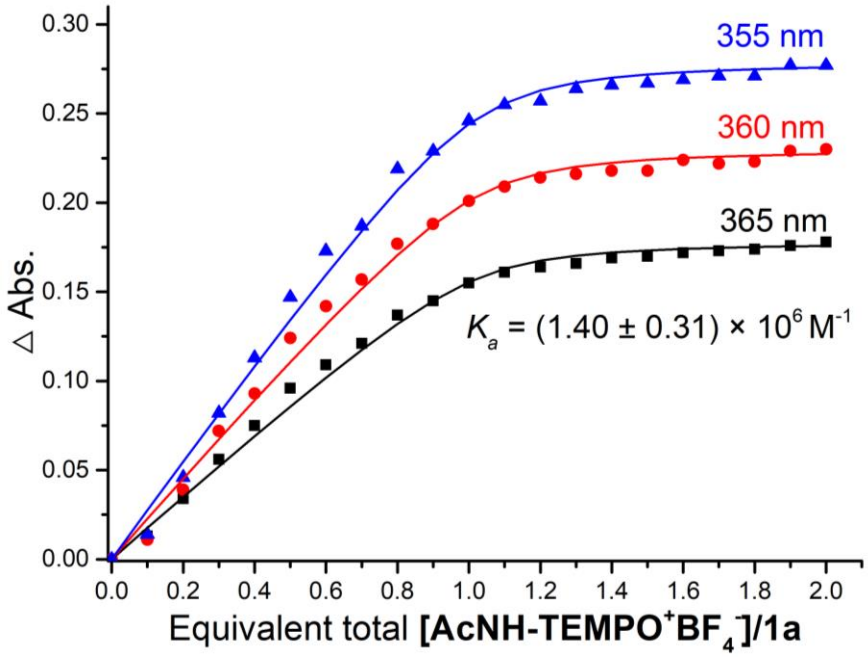

Figure S4 Curve fitting of the binding constant of **AcNH-TEMPO⁺BF₄⁻⊂1a** in $CHCl_3/CH_3CN$ (5:1, v/v, 298 K). The reported binding constant is the average value based on fitting of the absorbance at 355 nm, 360 nm and 365 nm.

^{1}H NMR spectra for 1a and AcNH-TEMPO$^+$BF$_4^-$ interactions

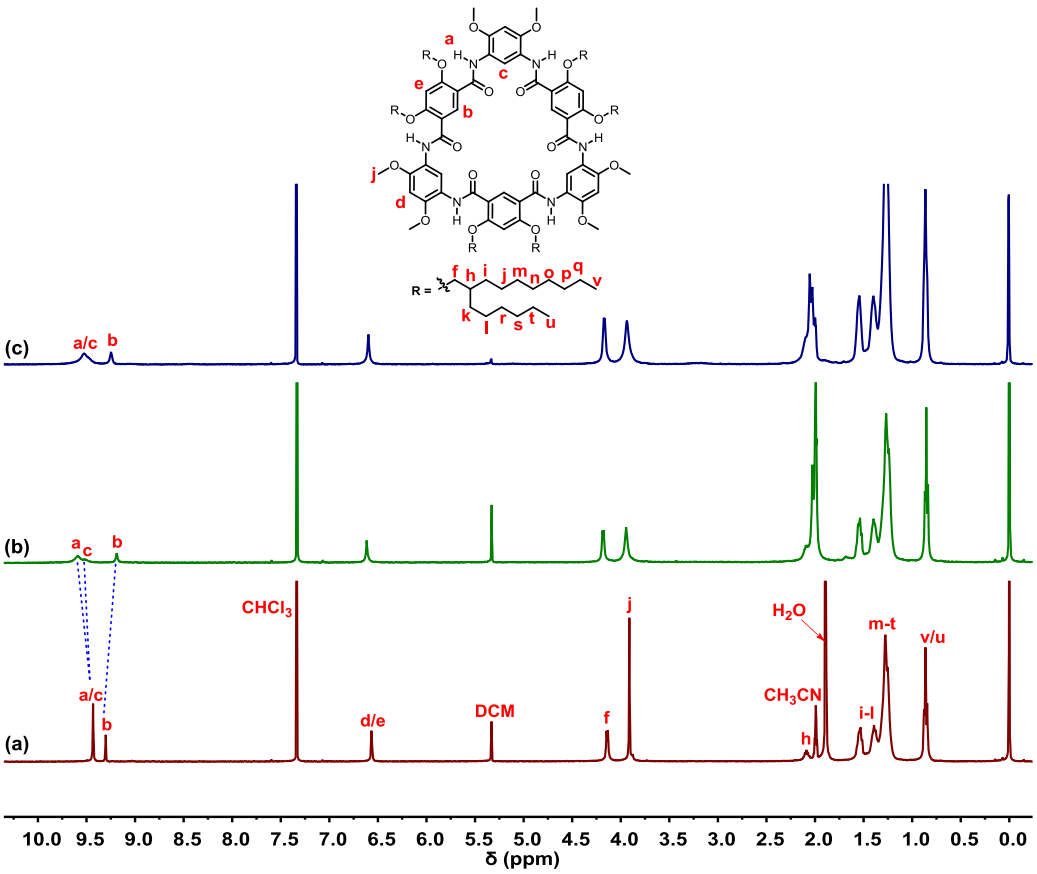

Figure S5 ^{1}H NMR spectra (400 MHz, $CDCl_3/CD_3CN$, 9:1, v/v 298 K) of (a) 1.0 mM **1a**, (b) 1.0 mM **1a** and 1.0 mM **AcNH-TEMPO$^+$BF$_4^-$**, (c) 2.0 mM **1a** and 1.0 mM **AcNH-TEMPO$^+$BF$_4^-$**.

Host-guest chemistry of 1a and AcNH-TEMPOH

Job plot for determination of stoichiometry

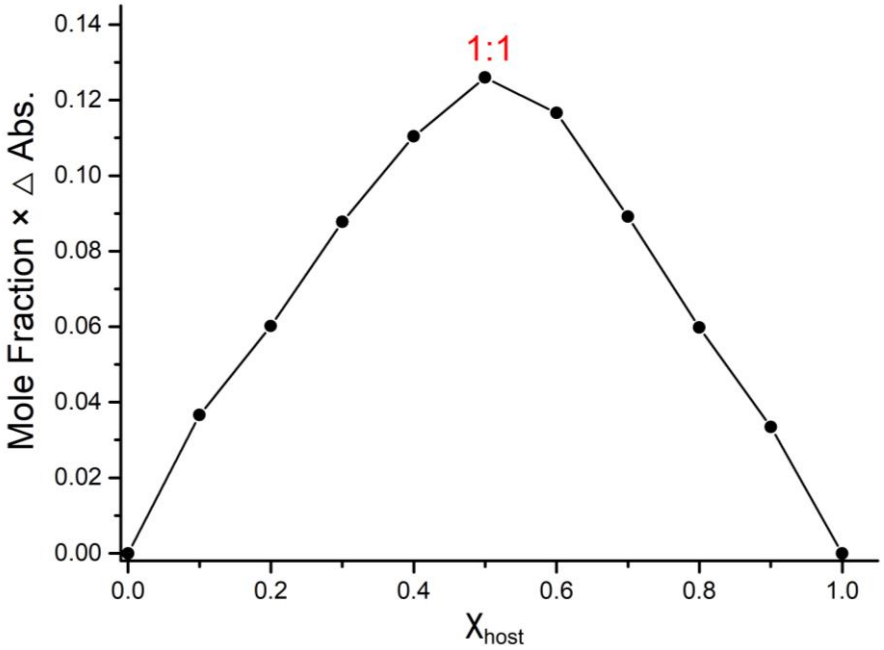

Figure S6 Job plot for determination of stoichiometry of **1a** and **AcNH-TEMPOH** based on the absorbance at 355 nm in $CHCl_3/CH_3CN$ (5:1, v/v, 298 K). [**1a**] + [**AcNH-TEMPOH**] = 50 μM.

MALDI-TOF-MS spectrum of AcNH-TEMPOH⊂1a

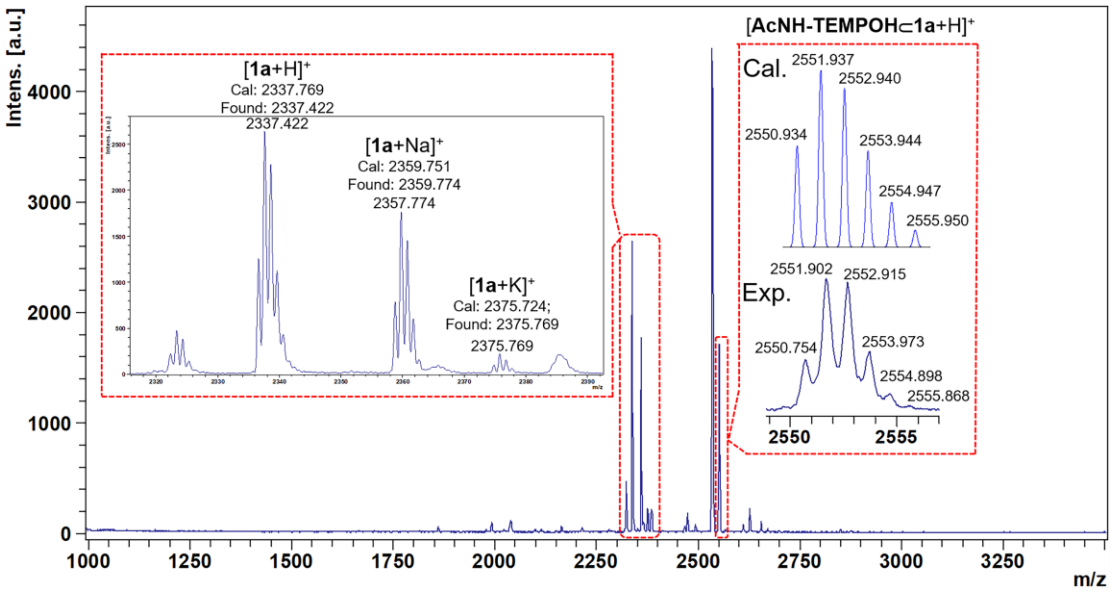

Figure S7 Full MALDI-TOF-MS spectrum of **AcNH-TEMPOH⊂1a** complex. MALDI-TOF-MS calculated for [**1a**+**AcNH-TEMPOH**+H]$^+$, m/z, 2551.937, found 2551.902.

UV-Vis titration experiments

To determinate the binding constant (K_a) of macrocycle **1a** and guest **AcNH-TEMPOH**, UV-vis titration experiments were performed in $CHCl_3/CH_3CN$ (5:1, v/v, 298 K) at a constant concentration of **1a** (50 μM) and varying concentration of **AcNH-TEMPOH**. For the titration, at least 20 data points were collected. Binding constant was calculated by a global fitting analysis according to a 1:1 binding model using the website *(http://supramolecular.org/)*.

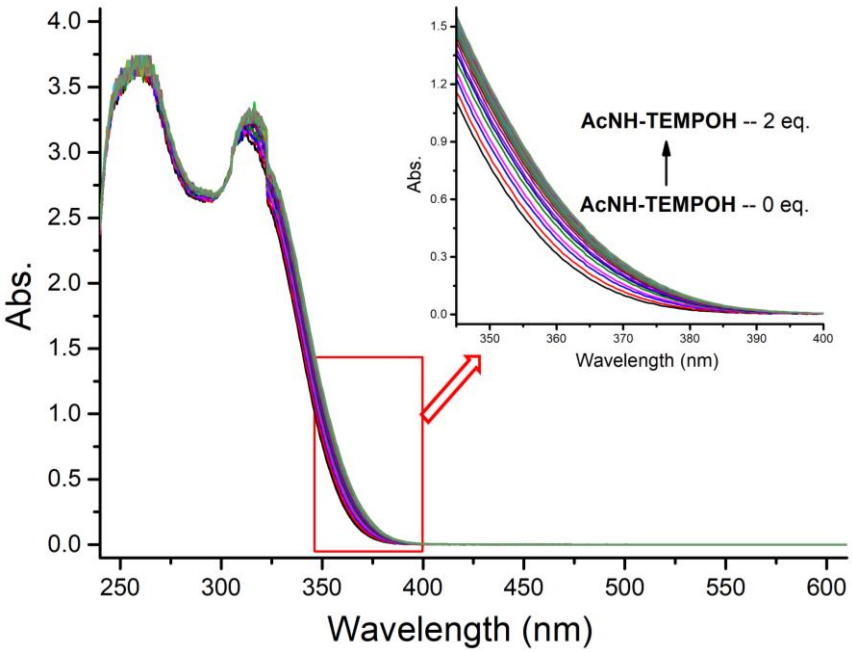

Figure S8 Stacked UV-Vis spectra of **1a** (50 μM) titrated with **AcNH-TEMPOH** in $CHCl_3/CH_3CN$ (5:1, v/v) at 298 K. Inserted are expended spectra in the wavelength range from 340 nm to 400 nm.

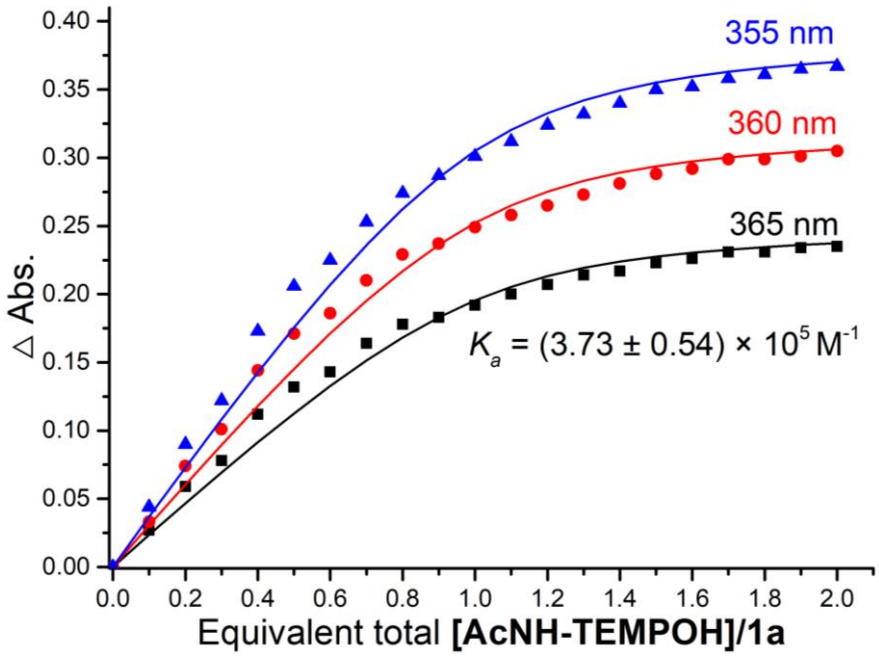

Figure S9 Curve fitting of the binding constant of **AcNH-TEMPOH⊂1a** in $CHCl_3/CH_3CN$ (5:1, v/v, 298 K). The reported binding constant is the average value based on fitting of the absorbance at 355 nm, 360 nm and 365 nm.

^{1}H NMR spectra of 1a and AcNH-TEMPOH

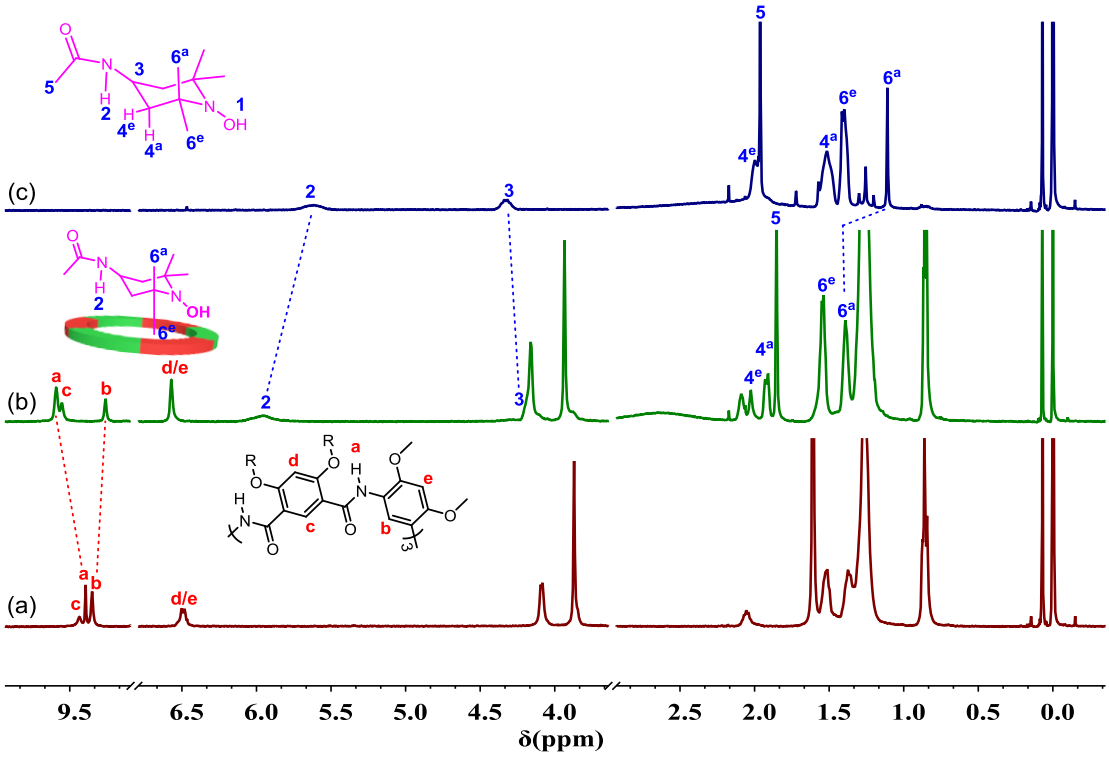

Figure S10 ^{1}H NMR spectra of (400 MHz, $CDCl_3$, 298 K) (a) 1 mM **1a** and excess $NaHCO_3$ (s), (b) **1a** and **AcNH-TEMPOH·HCl** in the presence of excess $NaHCO_3$ (s), (c) **AcNH-TEMPOH·HCl** in the presence of excess $NaHCO_3$ (s).

2D NOESY spectrum for AcNH-TEMPOH⊂1a

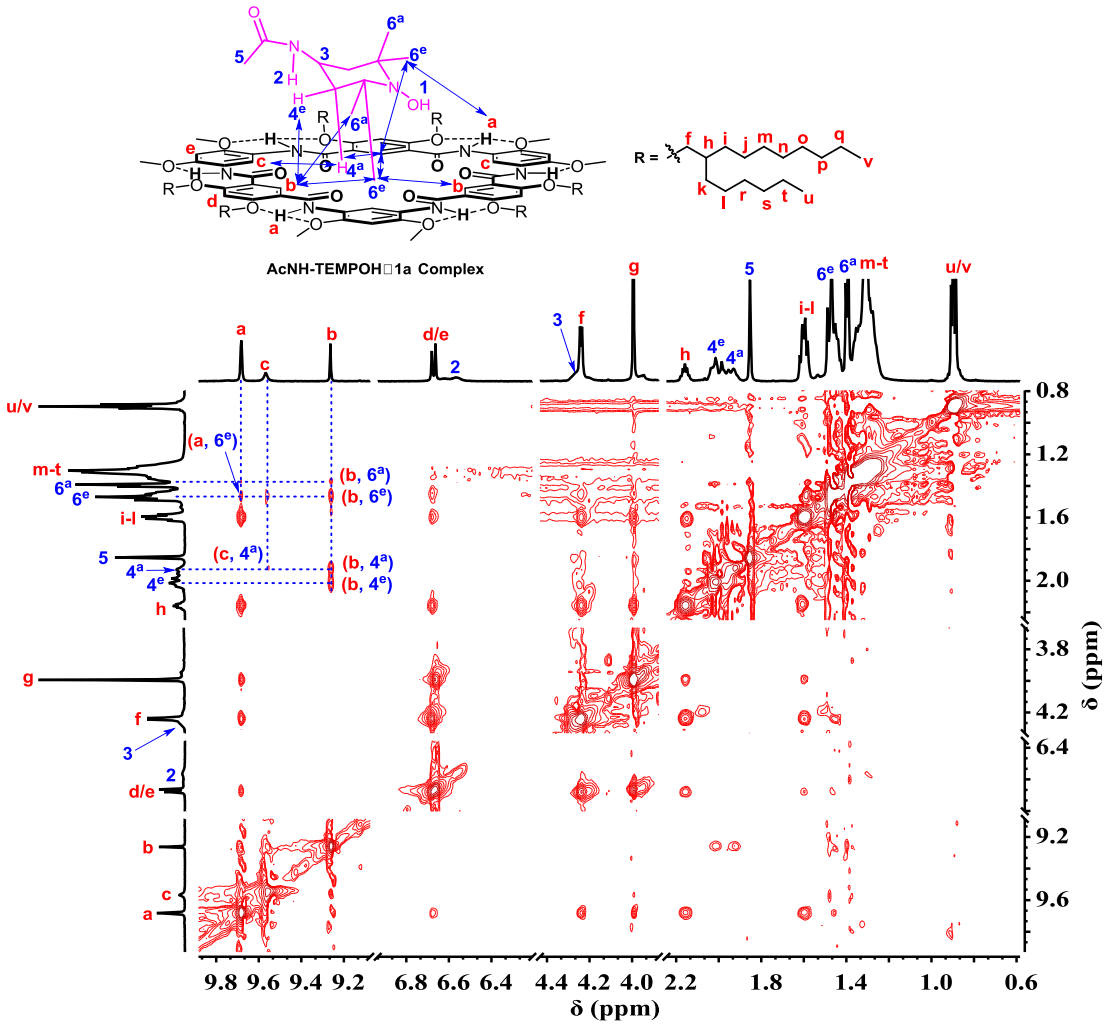

Figure S11 Expanded 2D-NOESY spectrum of **AcNH-TEMPOH⊂1a** (CD_2Cl_2, 298 K, 600 MHz, mixing time=0.4 s).

Oxidation reactions of unactivated alcohols in two-phase $H_2O/CDCl_3$ system

The standard Anelli's procedure for the biphasic catalytic oxidation of alcohols: [3] A solution of 0.1 M (1 equiv) alcohol in $CDCl_3$ (0.5 mL) was mixed with a buffer solution of 0.5 M $NaHCO_3$ (1 mL), following by addition of **AcNH-TEMPO$^+$BF$_4^-$** (2 mol %), or **AcNH-TEMPO$^+$BF$_4^-$⊂CB[7]** (2 mol %), or **AcNH-TEMPO$^+$BF$_4^-$⊂1a** (2 mol %). 60 μL of 1.13 M NaClO solution was then added dropwise. The reaction mixture was stirred at 25 ℃. Finally, the internal standard $CHCl_2CHCl_2$ (2.0 equiv) was added, and the mixture was stirred for 2 minutes. The $CDCl_3$ phase was collected into the NMR tube for the analysis of reaction yield.

Background reactions of without AcNH-TEMPO$^+$BF$_4^-$

No reactions were observed with benzyl alcohol and phenylpropanol in the absence of **AcNH-TEMPO$^+$BF$_4^-$**.

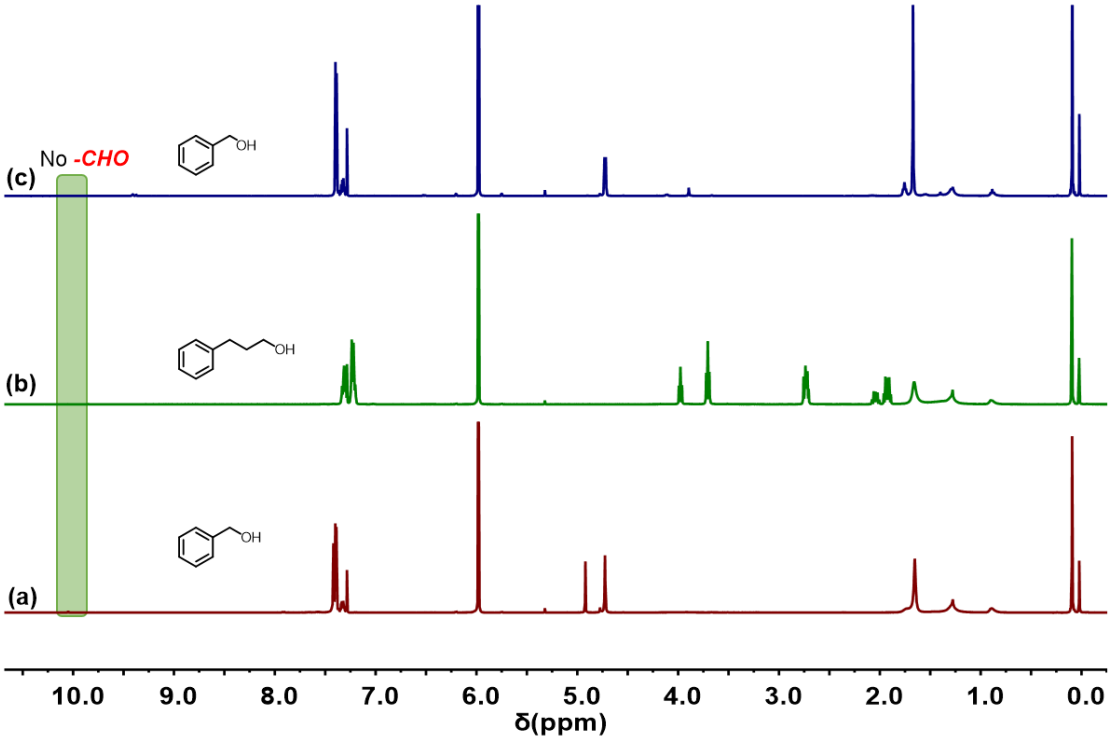

Figure S12 Background reactions of (a) benzyl alcohol and (b) phenylpropanol catalyzed by **1a** and NaClO; (c) benzyl alcohol catalyzed by NaClO alone.

Evaluation of the stability of AcNH-TEMPO$^+$BF$_4^-$

The procedure for evaluating the stability of AcNH-TEMPO$^+$BF$_4^-$ in the presence of NaClO (10 equiv) solution. To evaluate the stability of **AcNH-TEMPO$^+$BF$_4^-$**, the decay kinetic study on the oxidation process of **AcNH-TEMPO$^+$BF$_4^-$** was performed in the presence of NaClO (10 eq.). By monitoring the evolution of the UV-vis spectra, we found that the UV-vis absorbance gradually increases during the first 3 hours (Figure S13). The time-retention ratio relationship was plotted based on the absorption at 270 nm. The results indicated that **AcNH-TEMPO$^+$BF$_4^-$** decomposes rapidly in 3 h under the oxidation condition (Figure S14).

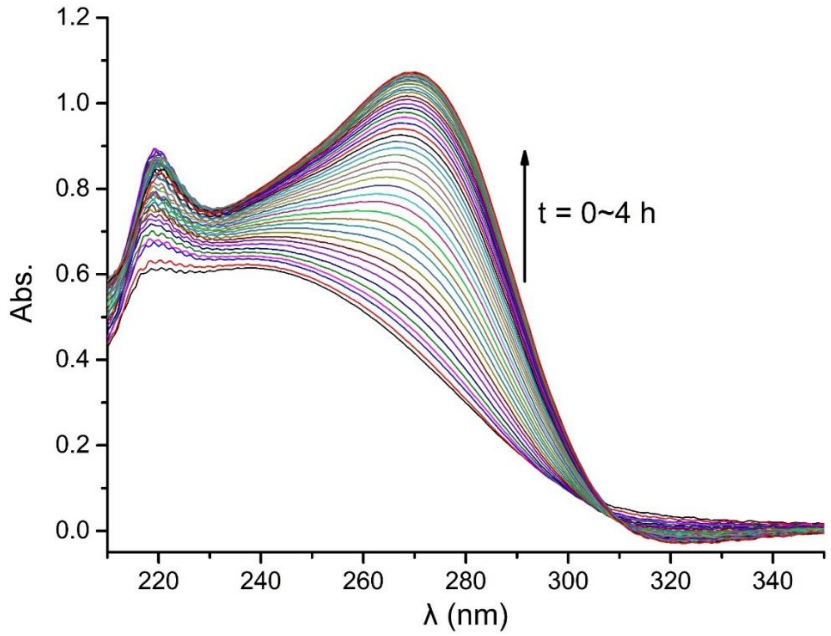

Figure S13 The evolutions of UV-vis spectra of **AcNH-TEMPO$^+$BF$_4^-$** in aqueous phase ($NaHCO_3$ buffer) in the presence of NaClO (10 equiv).

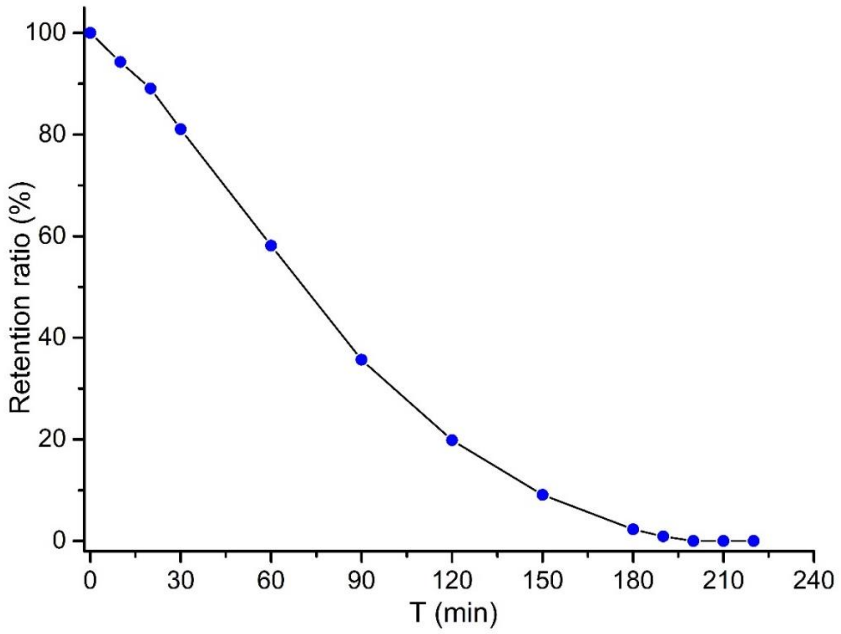

Figure S14 The stability of **AcNH-TEMPO$^+$BF$_4^-$** in aqueous phase ($NaHCO_3$ buffer) in the presence of NaClO (10 equiv) monitored by UV-vis spectroscopy. Results based on the absorbance at 270 nm.

The procedure for evaluating the stability of the complex AcNH-TEMPO$^+$BF$_4^-$⊂1a in the organic phase under oxidation conditions. To evaluate the stability of **AcNH-TEMPO$^+$BF$_4^-$⊂1a** in the organic under the oxidation condition**,** the kinetic study in biphasic $H_2O/CHCl_3$ system was performed. A mixture containing a solution of 3 mM **1a** in $CHCl_3$ (3 mL) and a solution of 3 mM **AcNH-TEMPO$^+$BF$_4^-$** in water (3 mL) was stirred at 25 ℃ for 5 min. **AcNH-TEMPO$^+$BF$_4^-$** was rapidly transferred by **1a** from the aqueous phase into the organic

phase. After centrifugation, 0.1 mL $CHCl_3$ was removed from the organic phase and transferred to a cuvette, and 2.9 mL $CHCl_3$ was added. The absorption was recorded for the final solution (Figure S15).

NaClO (10 eq.) was added to the above two-phase $H_2O/CHCl_3$ system, and then the mixture was stirred. At different time, 0.1 mL $CHCl_3$ was removed from the organic phase and transferred to a cuvette after centrifugation, and 2.9 mL $CHCl_3$ was added. The absorption was recorded for the final solution. The results shown in Figure S16 indicated that the absorbance of **AcNH-TEMPO$^+$BF$_4^-$⊂1a** is fluctuated in a certain range (0.702-0.810 at 365 nm) in the presence of excess NaClO. Therefore, we concluded that the complex **AcNH-TEMPO$^+$BF$_4^-$⊂1a** is stable in the organic phase under oxidation conditions for at least 4 h.

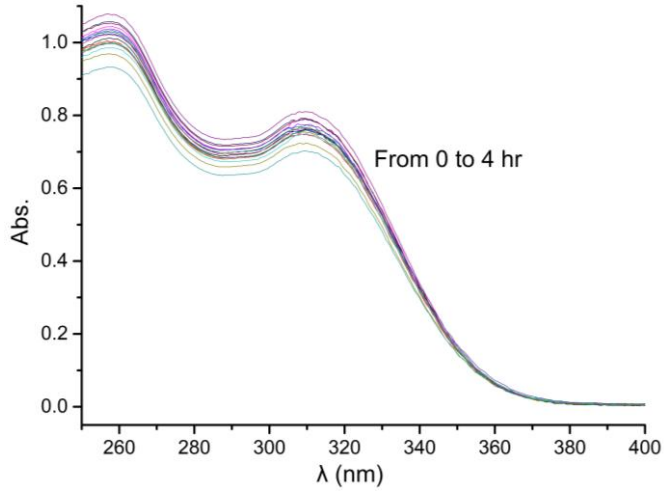

Figure S15 The evolution of UV-vis spectra of **AcNH-TEMPO$^+$BF$_4^-$⊂1a** in organic phase in the presence of NaClO from 0 to 4 h.

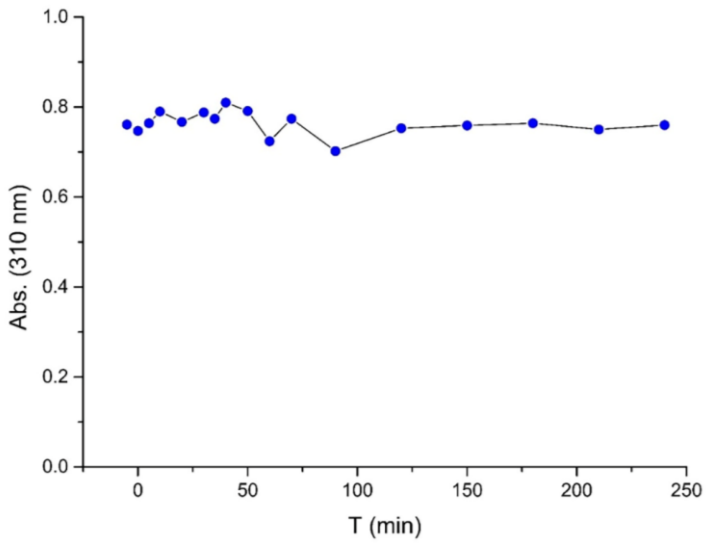

Figure S16 Time-absorbance curves for the complex **AcNH-TEMPO$^+$BF$_4^-$⊂1a**. Results based on the absorbance at 310 nm.

Phase transfer of AcNH-TEMPO$^+$BF$_4^-$ monitored by conductivity experiments

AcNH-TEMPO$^+$BF$_4^-$ has a much larger solubility in H_2O (11.5 g/100 mL) than in $CHCl_3$ (18 mg/100 mL).[4] The macrocycle **1a** is able to bind **AcNH-TEMPO$^+$** due to the presence of an electron-rich cavity, which has the ability

to transfer the cationic catalyst from the aqueous phase to the organic phase. The percentages of the transferred **AcNH-TEMPO$^+$BF$_4^-$** to the organic phase under the catalytic condition in the presence of different amount of **1a** can be estimated by conductivity experiments. First, the standard conductivity curve of **AcNH-TEMPO$^+$BF$_4^-$** was conducted (Figure S17). Then, 25 mL of $CHCl_3$ solution of **1a** (5 mM) was mixed with 25 mL of H_2O solution of **AcNH-TEMPO$^+$BF$_4^-$** (5 mM). The mixture was slightly stirred. The electrode was carefully soaked in the aqueous solution above without touching the organic phase below. The amount of the decrease of monitored conductivity was contributed by the transferred **AcNH-TEMPO$^+$BF$_4^-$**. As shown in Figure S18, the percentage of transferred **AcNH-TEMPO$^+$BF$_4^-$** was calculated to be ~17% in the presence of **1a** (1 equiv) until the phase transfer reached the equilibrium.

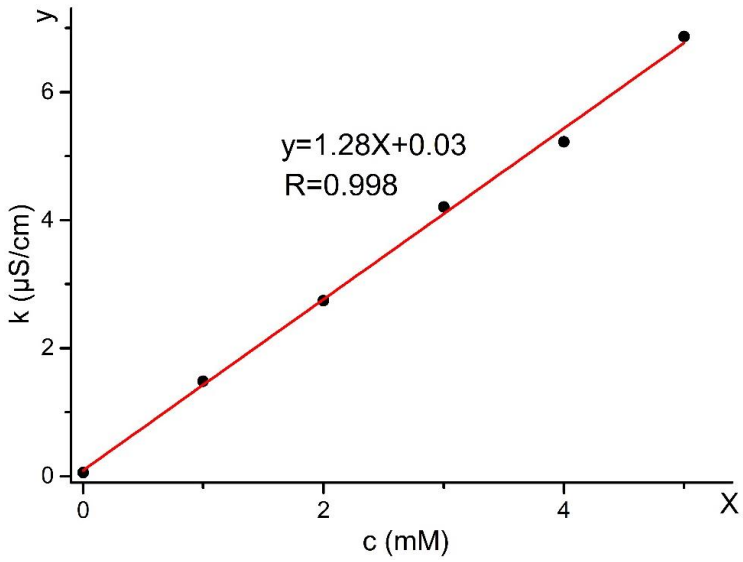

Figure S17 . Standard conductivity curve of **AcNH-TEMPO$^+$BF$_4^-$** in water.

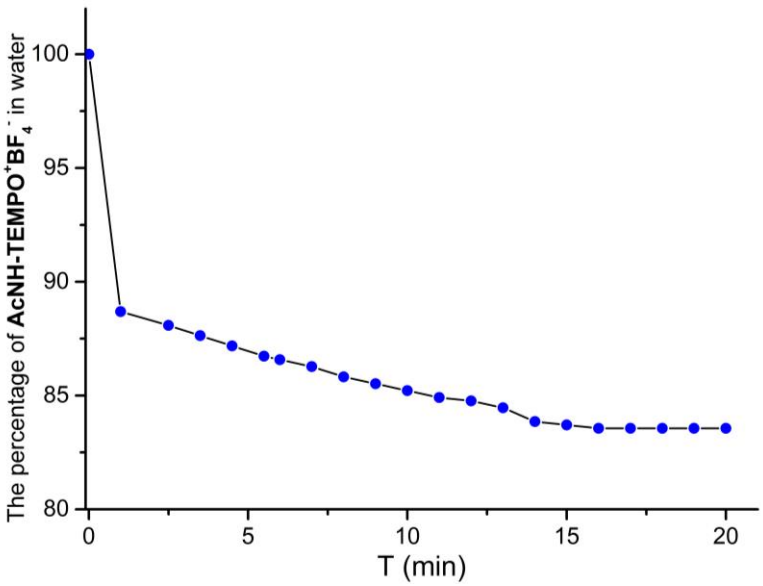

Figure S18 Time-dependent percentage curves for the **AcNH-TEMPO$^+$BF$_4^-$** in water in the presence of **1a**.

Phase transfer of AcNH-TEMPOH monitored by ^{1}H NMR experiments

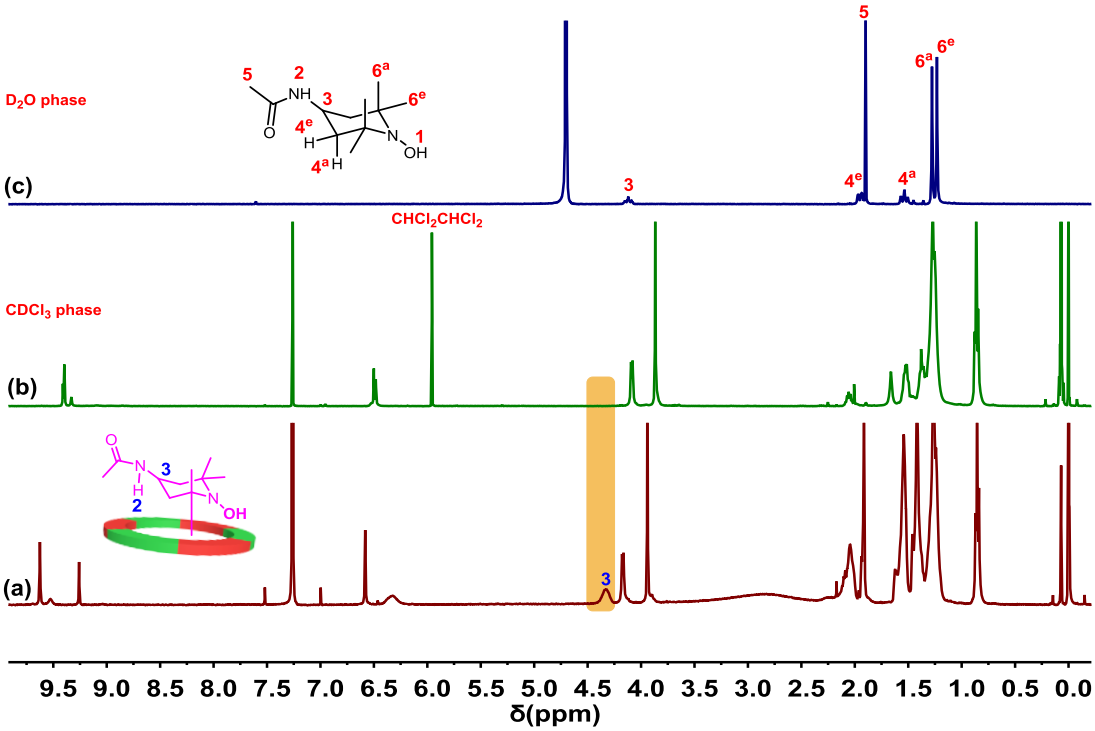

Figure S19 ^{1}H NMR spectra of (400 MHz, 298 K) a) the mixture of 1.0 mM **AcNH-TEMPOH** and 1.0 mM **1a** in $CDCl_3$ before adding D_2O, b) $CDCl_3$ phase after adding D_2O to the solution above, and c) D_2O Phase after adding D_2O to the solution above. $CHCl_2CHCl_2$ was used as an internal standard.

Apparent kinetics of the catalytic biphasic oxidation

The apparent kinetics of the biphasic catalytic oxidation were measured using phenylproanol as a model substrate. As shown in **Figure S20-S21**, the oxidation process was nearly completed about 2 hr. The oxidation catalyzed by **AcNH-TEMPO$^+$BF$_4^-$⊂1a** displayed a faster reaction rate with a higher final conversion than that by using **AcNH-TEMPO$^+$BF$_4^-$** alone.

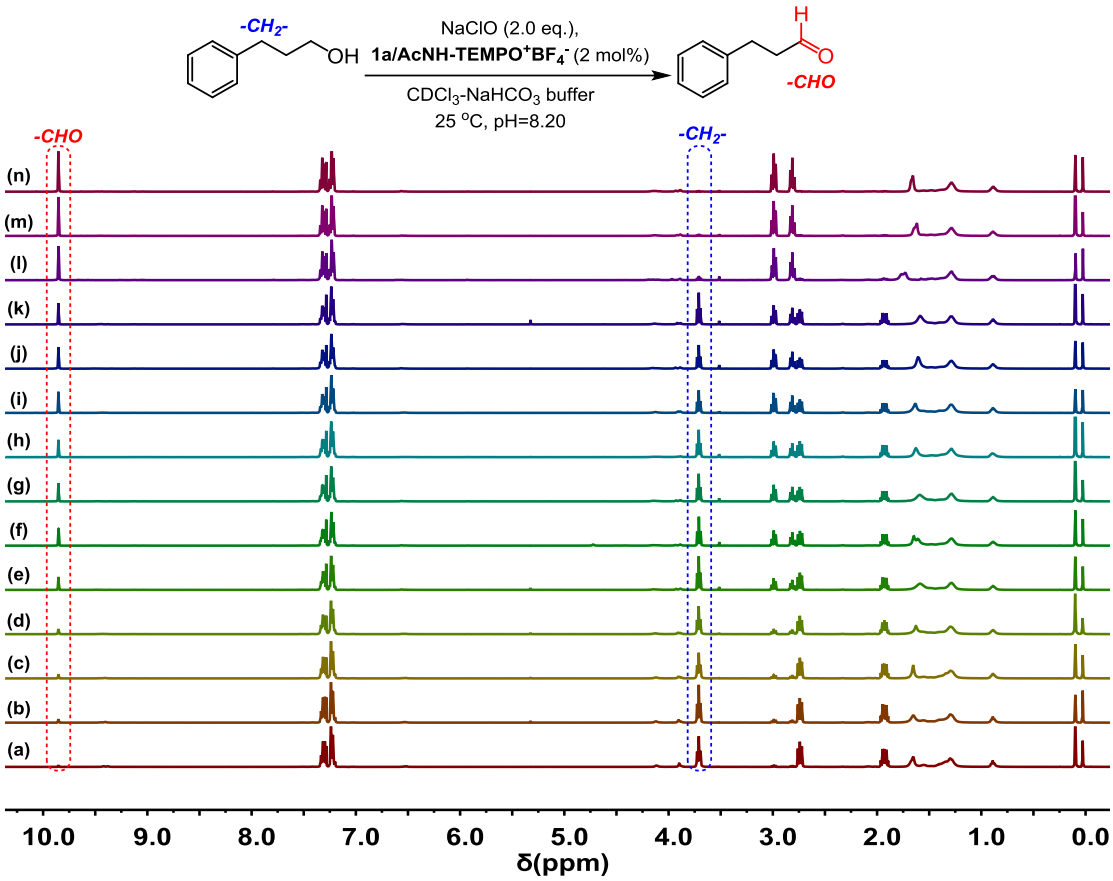

Figure S20 Stacked ^{1}H NMR spectra (400 MHz, $CDCl_3$, v/v, 298 K) of the biphasic oxidation of phenylproanol catalyzed by **AcNH-TEMPO^{+}BF$_4^{-}$⊂1a**. The spectra from bottom to top correspond to the reaction at (a) 1 min, (b) 3 min, (c) 5 min, (d) 7 min, (e) 10 min, (f) 15 min, (g) 20 min, (h) 30 min, (i) 40 min, (j) 50 min, (k) 60 min, (l) 80 min, (m) 100 min, (n) 120 min.

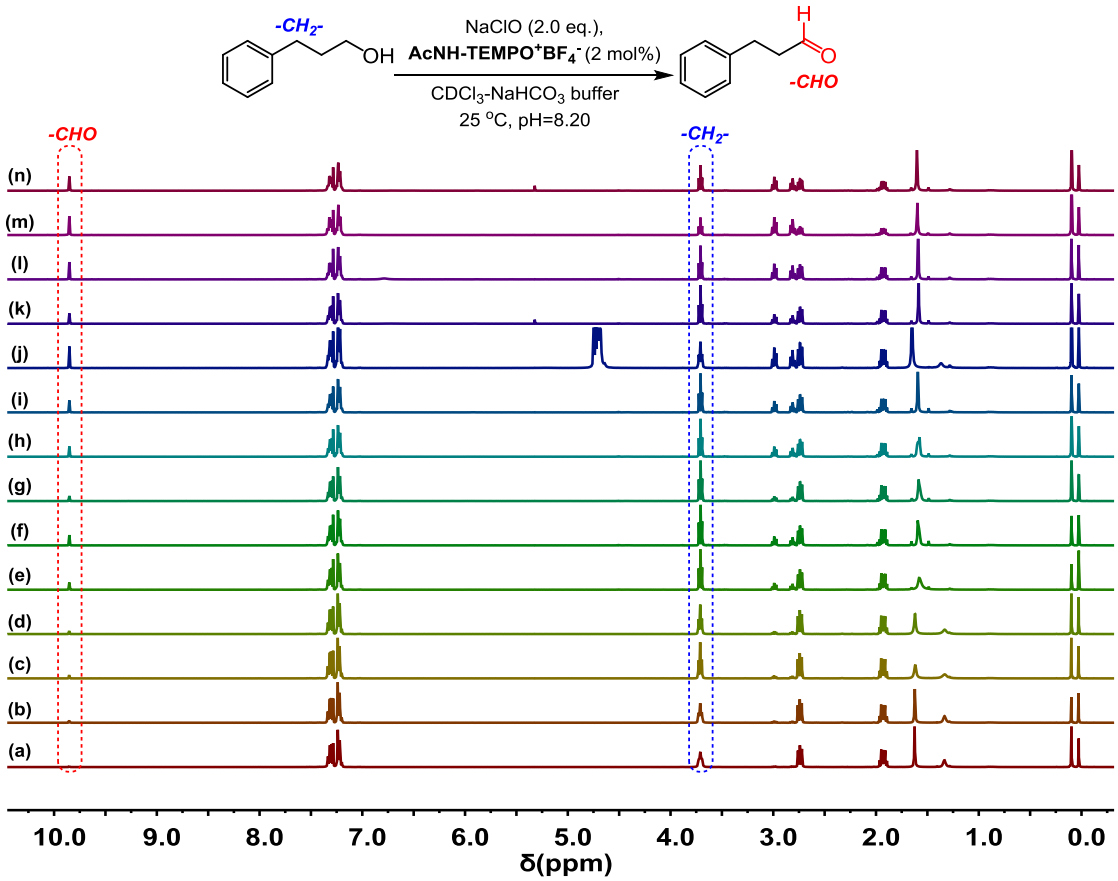

Figure S21 Stacked ^{1}H NMR spectra (400 MHz, $CDCl_3$, v/v, 298 K) of conversions of biphasic oxidation of phenylproanol catalyzed by **AcNH-TEMPO$^+$BF$_4^-$**. The spectra from bottom to top correspond to the reaction at (a) 1 min, (b) 3 min, (c) 5 min, (d) 7 min, (e) 10 min, (f) 15 min, (g) 20 min, (h) 30 min, (i) 40 min, (j) 50 min, (k) 60 min, (l) 80 min, (m) 100 min, (n) 120 min.

Table S1 Kinetic study of biphasic oxidation catalyzed by **AcNH-TEMPO$^+$BF$_4^-$⊂1a** or **AcNH-TEMPO$^+$BF$_4^-$**

Entry	Time (min)	[Phenylproanol] (C_a, mol/L)		Ln ($C_{a,0}$ / C_a) [a]	
		With **1a**	Without **1a**	With **1a**	Without **1a**
a	1	0.0982	0.1003	0.0769	0.0555
b	3	0.0930	0.0964	0.1312	0.0954
c	5	0.0867	0.0936	0.2009	0.1244
d	7	0.0789	0.0894	0.2957	0.1708
e	10	0.0688	0.0847	0.4323	0.2244
f	15	0.0602	0.0789	0.5656	0.2957
g	20	0.0530	0.0742	0.6931	0.3567

[a] $C_{a,0}$=0.106 mol/L.

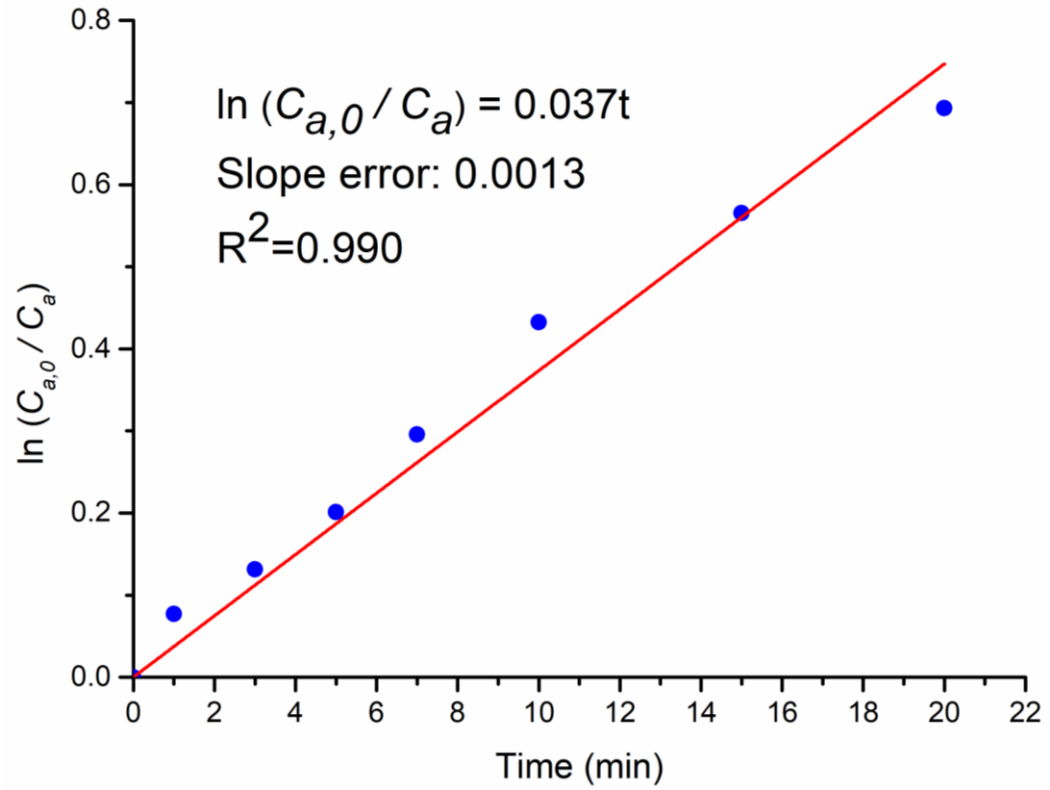

Figure S22 Linear curve fitting of the concentration of phenylproanol against reaction time, indicating a pseudo first order dependence of the reaction rate on phenylproanol.

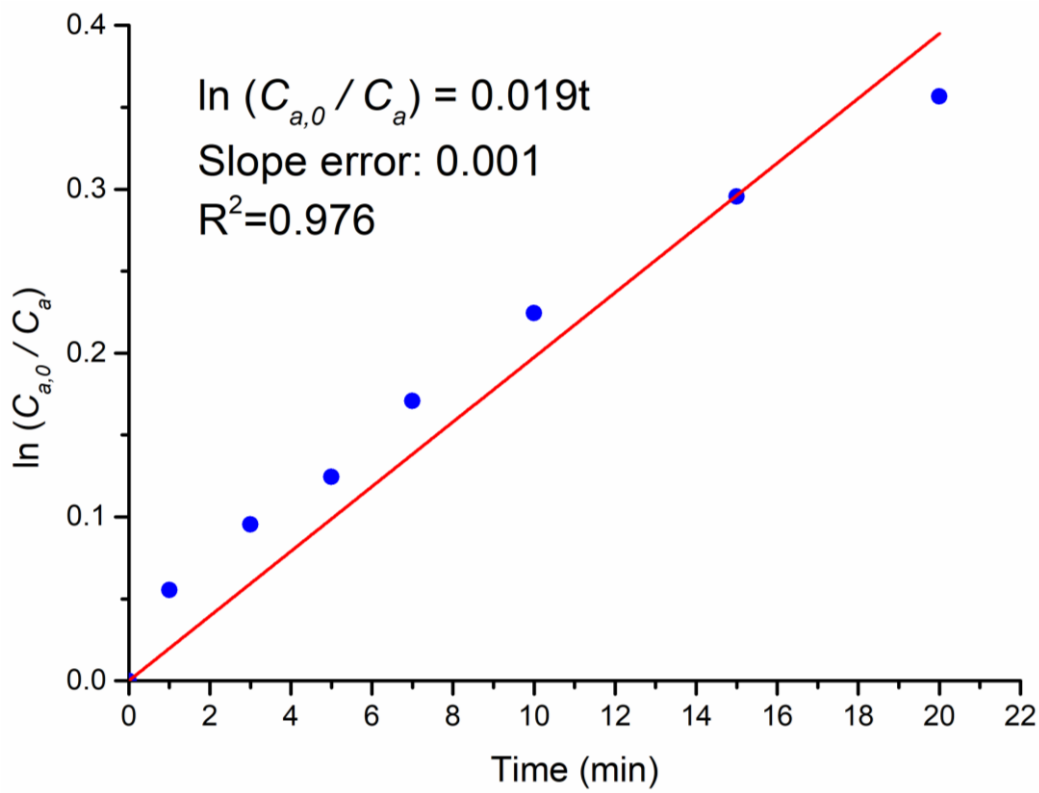

Figure S23 Linear curve fitting of the concentration of phenylproanol against reaction time, indicating a pseudo first order dependence of the reaction rate on phenylproanol.

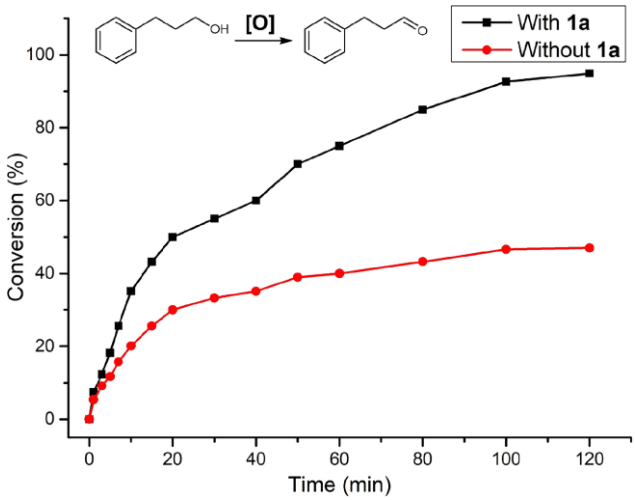

Figure S24 The time-conversion relationships of the biphasic oxidation using phenylpropanol as the substrate catalyzed by **AcNH-TEMPO$^+$BF$_4^-$** and **AcNH-TEMPO$^+$BF$_4^-$ ⊂ 1a**, respectively.

Turnover number of AcNH-TEMPO$^+$BF$_4^-$ ⊂ 1a

A solution of 0.1 M (1 eq.) alcohol (phenylpropanol and benzyl alcohol) in $CDCl_3$ (0.5 mL) was mixed with a buffer solution of 0.5 M $NaHCO_3$ (1 mL), following by addition of **AcNH-TEMPO$^+$BF$_4^-$ ⊂ 1a** (0.5 mol %). 60 μL of 1.13 M NaClO was then added dropwise. The reaction mixture was stirred at 25 ℃ for 2 h. Finally, the $CDCl_3$ phase was collected for ^{1}H NMR analysis of the reaction conversions. No side products were observed from the ^{1}H NMR results.

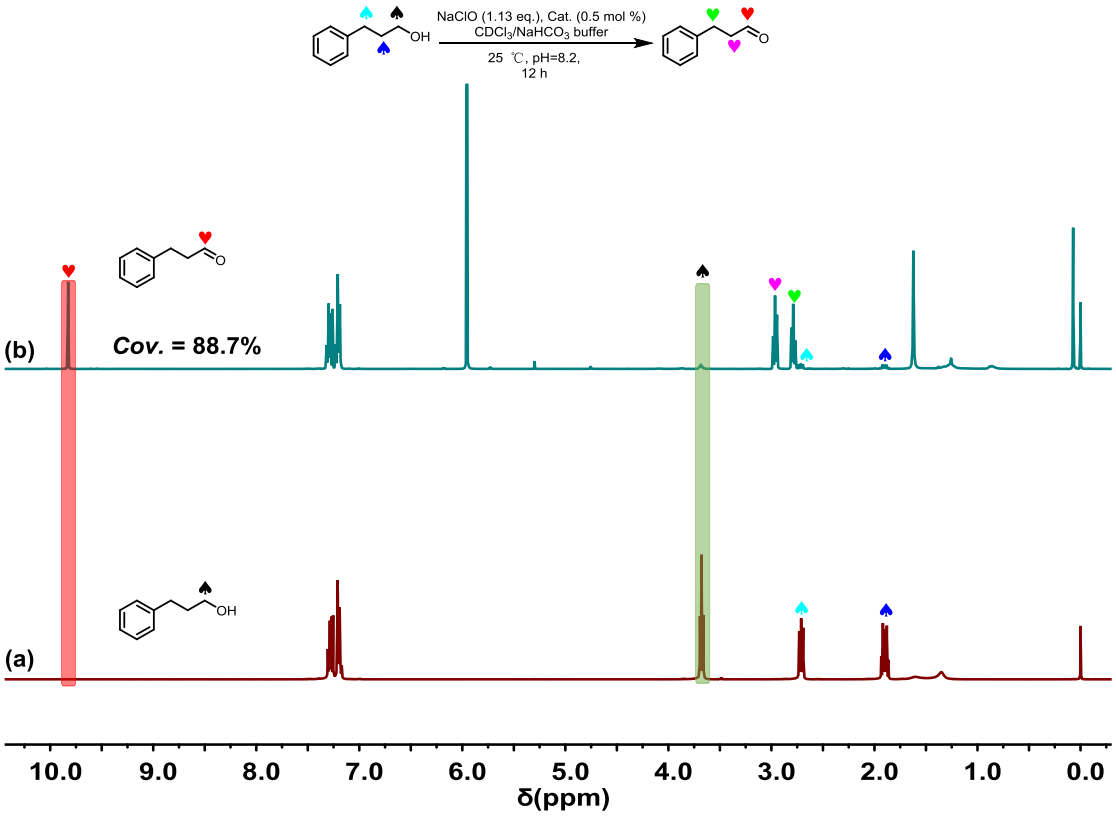

Figure S25 Stacked ^{1}H NMR spectra (400 MHz, $CDCl_3$, v/v, 298 K) of (a) phenylpropanol, (b) the conversions of biphasic oxidation of

phenylpropanol catalyzed by **AcNH-TEMPO$^+$BF$_4^-$⊂1a** (0.5 mol%).

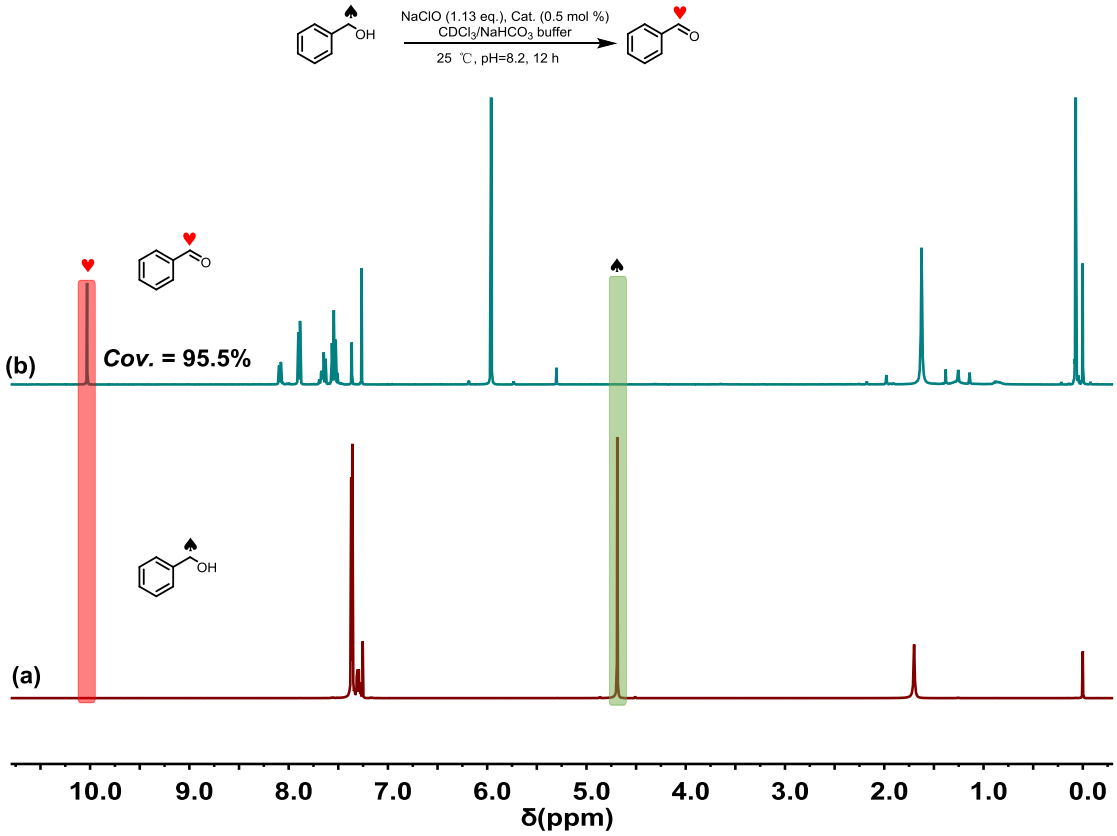

Figure S26 Stacked ^{1}H NMR spectra (400 MHz, $CDCl_3$, v/v, 298 K) of (a) benzyl alcohol, (b) the conversions of biphasic oxidation of benzyl alcohol catalyzed by **AcNH-TEMPO$^+$BF$_4^-$⊂1a** (0.5 mol%).

Apparent kinetics of the monophasic oxidation

As shown in Figure S26-S32, the apparent kinetics of the oxidation in organic phase was measured with benzyl alcohol and phenylpropanol as model substrates. ^{1}H NMR yields of the products were determined using 1,1,2,2-tetrachloroethane as an internal standard. The oxidation catalyzed by **AcNH-TEMPO$^+$BF$_4^-$⊂1a** displayed a faster reaction rate than that by the free catalyst **AcNH-TEMPO$^+$BF$_4^-$**.

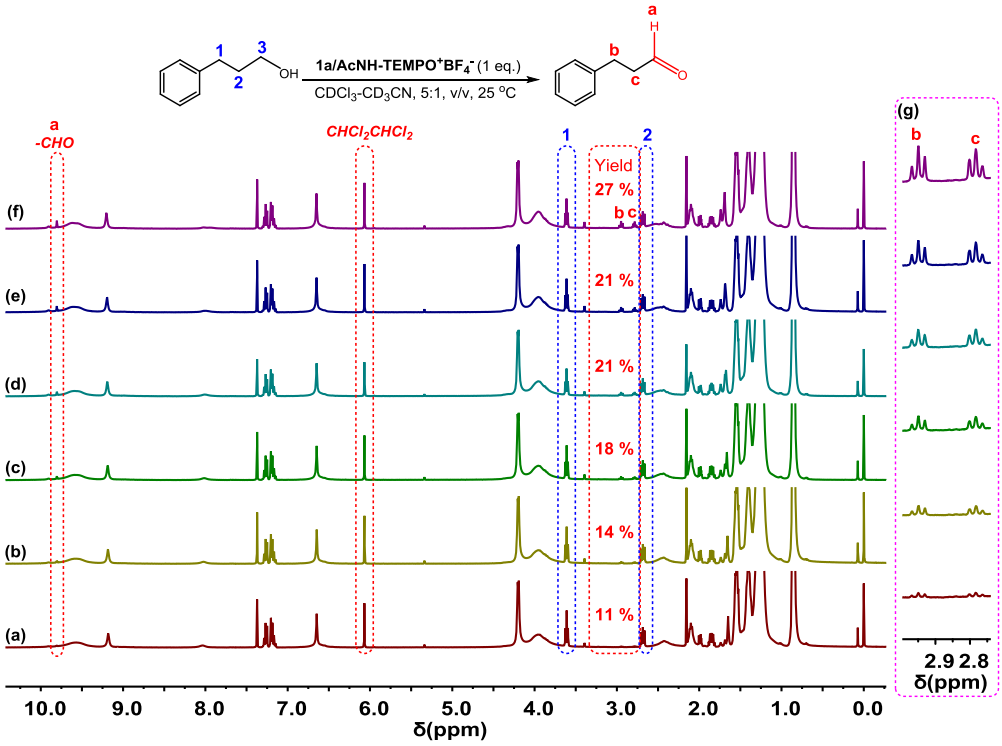

Figure S27 Stacked ^{1}H NMR spectra (400 MHz, $CDCl_3$-CD_3CN, 5;1, v/v, 298 K) of yields of monophasic oxidation of phenylpropanol catalyzed by **AcNH-TEMPO$^+$BF$_4^-$⊂1a**. The spectra from bottom to top correspond to the reaction at (a) 5 min, (b) 12 min, (c) 25 min, (d) 40 min, (e) 50 min, (f) 120 min. (g) Zoomed ^{1}H NMR spectra of for protons *b* and *c* during catalysis.

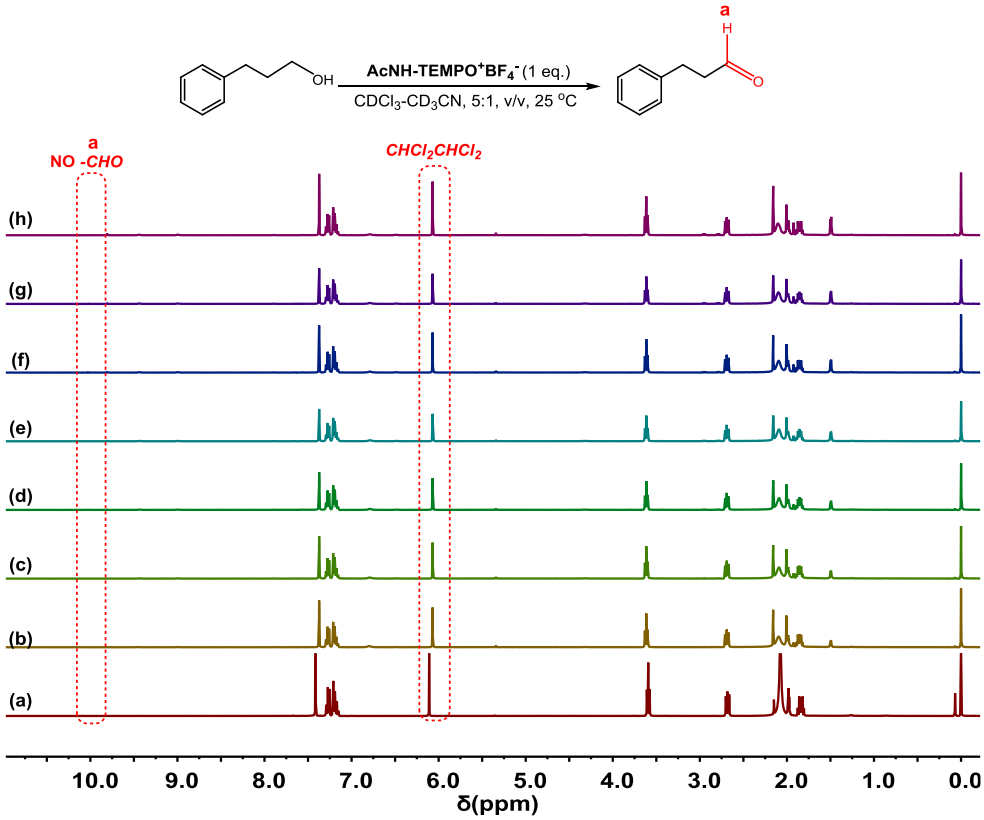

Figure S28 Stacked ^{1}H NMR spectra (400 MHz, $CDCl_3$-CD_3CN, 5;1, v/v, 298 K) of yields of monophasic oxidation of phenylpropanol catalyzed by **AcNH-TEMPO$^+$BF$_4^-$**. The spectra from bottom to top correspond to the reaction at (a) 0 min, (b) 5 min, (c) 12 min, (d) 24 min, (e) 36 min, (f) 60 min, (g) 70 min, (i) 120 min.

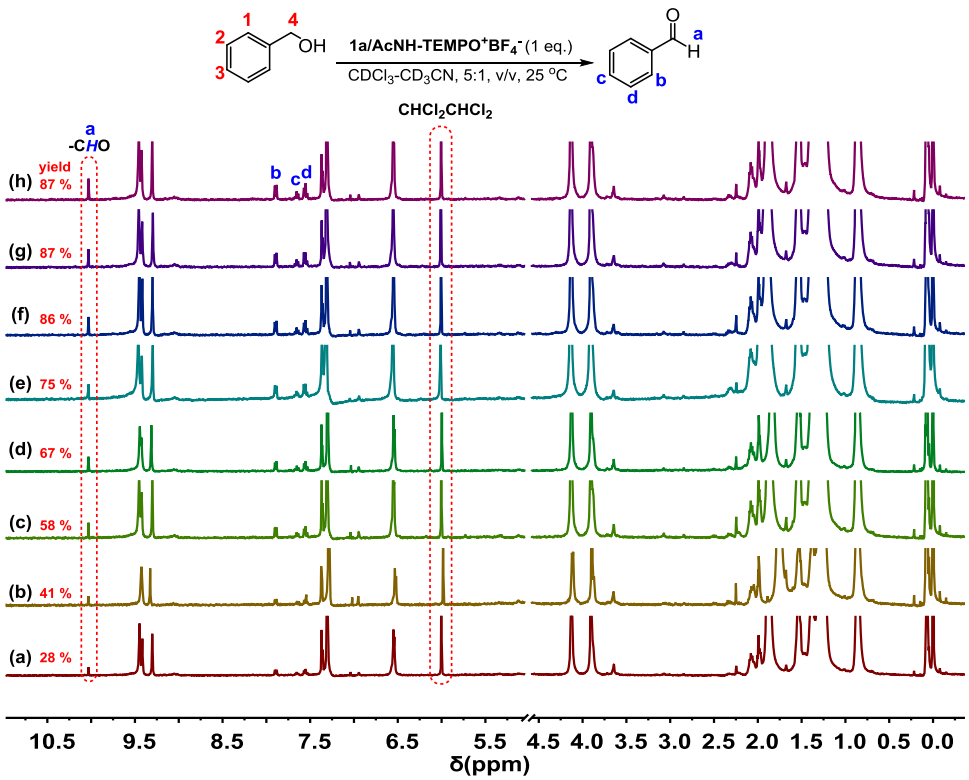

Figure S29 Stacked ^{1}H NMR spectra (400 MHz, $CDCl_3/CD_3CN$, 5;1, v/v, 298 K) of oxidation reaction of benzyl alcohol using **AcNH-TEMPO$^+$BF$_4^-$⊂1a** as catalyst after adding benzyl alcohol at (a) 2 min, (b) 4 min, (c) 6 min, (d) 8 min, (e) 10 min, (f) 12 min, (g) 14 min, and (h) 20 min. $CHCl_2CHCl_2$ was used as an internal standard.

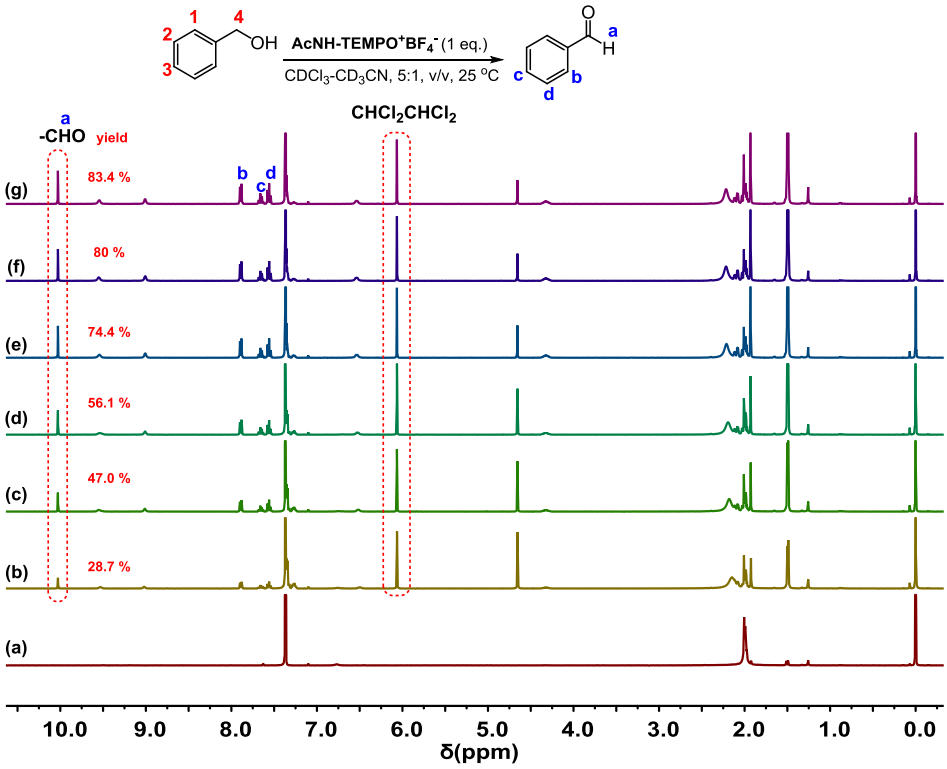

Figure S30 Stacked ^{1}H NMR spectra (400 MHz, $CDCl_3/CD_3CN$, 5;1, v/v, 298 K) of oxidation reaction of benzyl alcohol using **AcNH-TEMPO$^+$BF4$^-$⊂1a** as catalyst after adding benzyl alcohol at (a) 0 min (b) 4 min, (c) 10 min, (d) 15 min, (e) 37 min, (f) 48 min, (g) 64 min. $CHCl_2CHCl_2$ was used as an internal standard.

Table S2 Kinetic study of monophasic oxidation catalyzed by **AcNH-TEMPO$^+$BF$_4^-$⊂1a**

Time (min)	Benzyl alcohol C_a (mol/L)	ln ($C_{a,0}/C_a$)
0	0.00209	0
2	0.001505	0.328504
4	0.001233	0.527633
6	0.000878	0.867501
8	0.00069	1.108663
10	0.000523	1.386294
12	0.000293	1.966113

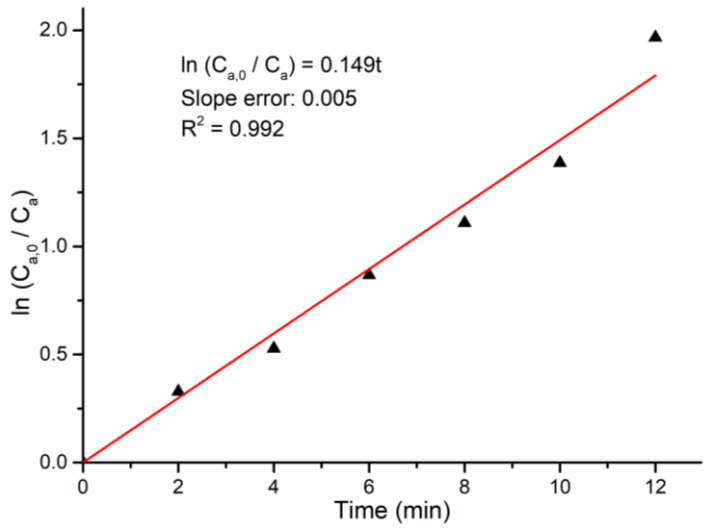

Figure S31 Linear curve fitting of the concentration of benzyl alcohol against reaction time, indicating a pseudo first-order kinetic of the reaction rate on benzyl alcohol.

Table S3 Kinetic study of monophasic oxidation catalyzed by **AcNH-TEMPO$^+$BF$_4^-$**

Time (min)	Benzyl alcohol C_a (mol/L)	Ln ($C_{a,0}/C_a$)
0	0.0152	0
4	0.0108	0.35
10	0.0081	0.63
15	0.0067	0.82
37	0.0039	1.33
48	0.0030	1.61
64	0.0025	1.80

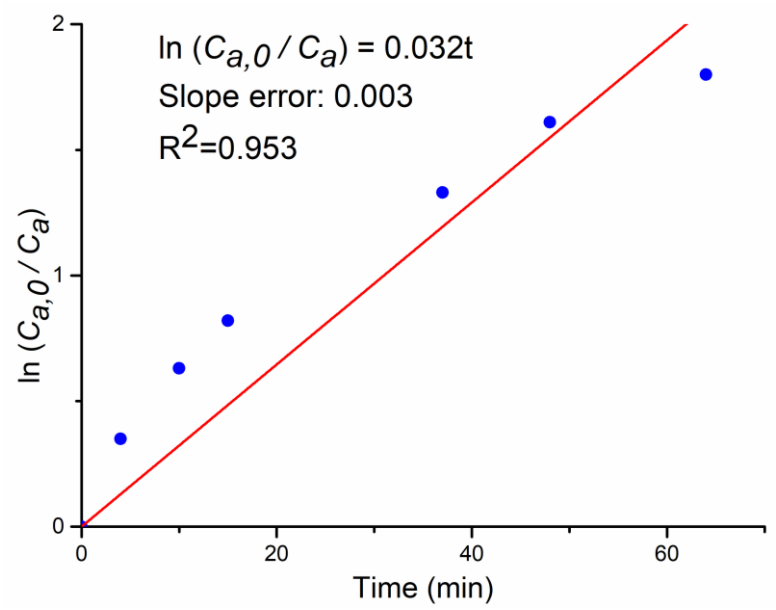

Figure S32 Linear curve fitting of the concentration of benzyl alcohol against reaction time, indicating a pseudo first-order dependence of the reaction rate on benzyl alcohol.

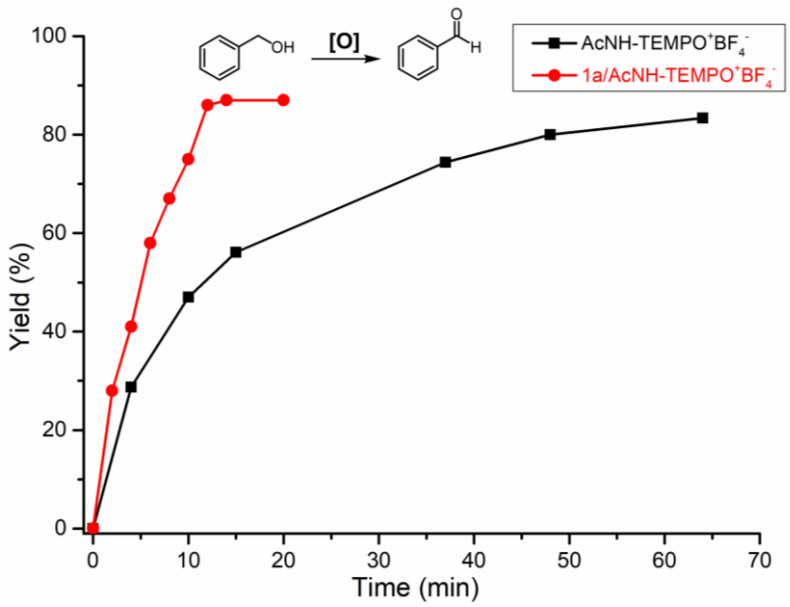

Figure S33 The time-yield relationship of the oxidation of benzyl alcohol catalyst by **AcNH-TEMPO$^+$BF$_4^-$** and **AcNH-TEMPO$^+$BF$_4^-$⊂1a**, respectively. The yields were determined by ^{1}H NMR analysis using $CHCl_2CHCl_2$ as internal standard.

X-ray crystal structure of AcNH-TEMPO$^+$BF$_4^-$⊂1b

Crystallographic data (excluding structure factors) for **AcNH-TEMPO$^+$BF$_4^-$⊂1b** reported in this communication have been deposited with the Cambridge Crystallographic Data Centre as supplementary publication no. CCDC–2039200. Data collection and structure refinement details can be found in the CIF files or obtained free of charge via *www.ccdc.cam.ac.uk/data_request/cif*.

Table S4 Crystallographic data and structure refinement for **AcNH-TEMPO$^+$BF$_4^-$⊂1b**

Identification code	**AcNH-TEMPO$^+$BF$_4^-$⊂1b**
CCDC No.	2039200
Empirical formula	$C_{200}H_{293}B_2F_8N_{22}O_{45}$
Formula weight	3899.20
Temperature/K	100.00 (10)
Crystal system	monoclinic
Space group	*P2$_1$/c*
a/Å	23.8670 (3)
b/Å	20.5849 (3)
c/Å	23.4795 (3)
α/°	90
β/°	117.284 (3)
γ/°	90
Volume/Å^3	10252.1 (3)
Z	2
ρ_{calc}g/cm^3	1.263
μ/mm^{-1}	0.775
F(000)	4178.0
Crystal size/mm^3	0.22 × 0.2 × 0.18
Radiation	CuKα (λ = 1.54184)
2Θ range for data collection/°	4.166 to 154.568
Index ranges	-29 ≤ h ≤ 30, -25 ≤ k ≤ 25, -29 ≤ l ≤ 22
Reflections collected	83534
Independent reflections	20836 [R_{int} = 0.0396, R_{sigma} = 0.1427]
Data/restraints/parameters	20836/717/1390
Goodness-of-fit on F^2	0.927
Final R indexes [I>=2σ (I)]	R_1 = 0.0930, wR_2 = 0.2433
Final R indexes [all data]	R_1 = 0.1390, wR_2 = 0.2627
Largest diff. peak/hole / e Å^{-3}	0.73/-0.72

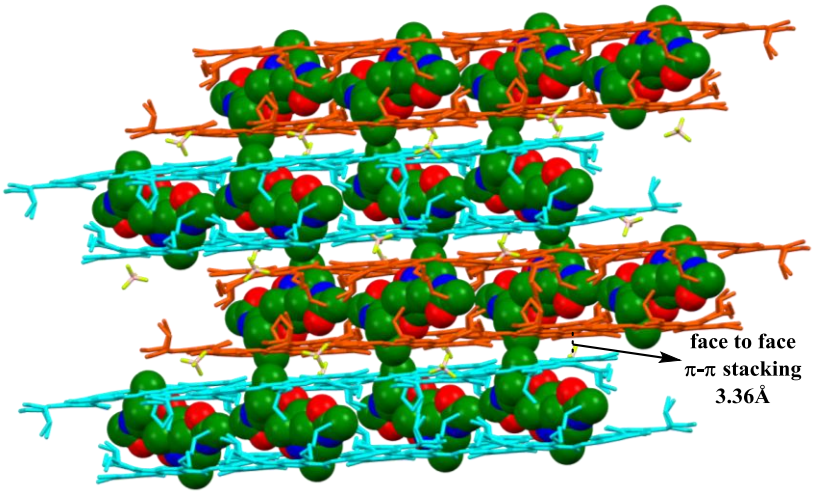

Figure S34 Crystal packing structure of **AcNH-TEMPO$^+$BF$_4^-$⊂1b**. BF_4^- counterions and all hydrogen atoms were omitted for clarity.

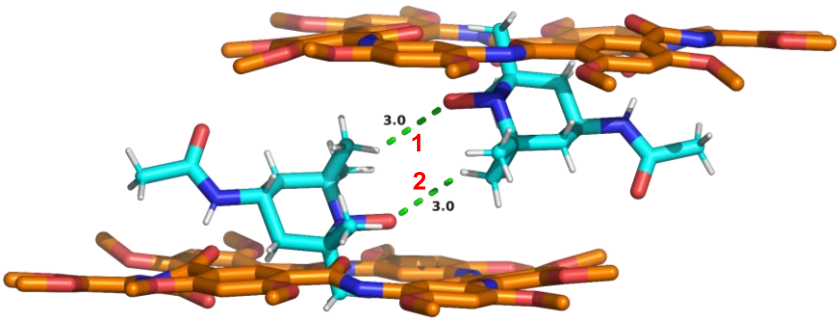

Figure S35 Hydrogen bonding between the two cationic guests (**AcNH-TEMPO$^+$BF$_4^-$**). The side chains and hydrogen atoms of **1b** were omitted for clarity (C orange and cyan, O red, N blue, H white).

Table S5 C-H···O hydrogen bonds between the two cationic guests **AcNH-TEMPO$^+$BF$_4^-$**

No. of C-H···O interaction	H···O / Å C-H···O angles	No. of C-H···O interaction	H···O / Å C-H···O angles
1	2.97 Å (136.3°)	2	2.97 Å (136.3°)

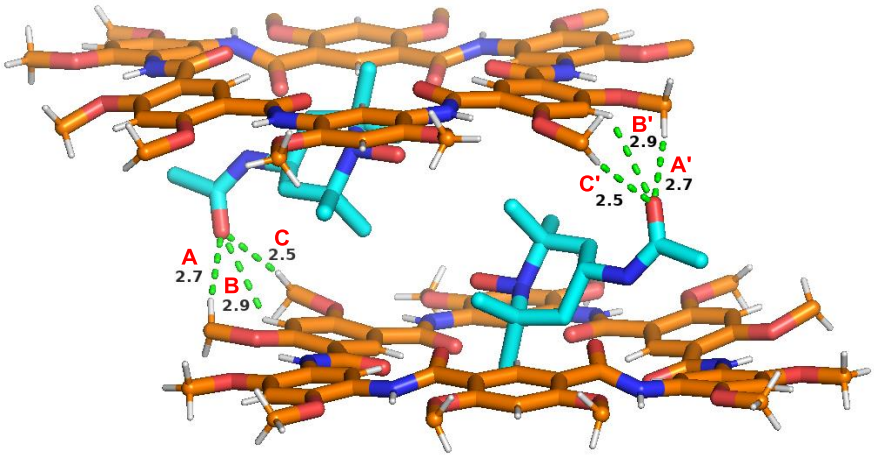

Figure S36 H-bonds between the carbonyl oxygens of **AcNH-TEMPO$^+$BF$_4^-$** and the side chains of **1b**. The side chains and part hydrogen atoms were omitted for clarity (C orange and cyan, O red, N blue, H white).

Table S6 C-H···O hydrogen bonds between the carbonyl oxygens of **AcNH-TEMPO$^+$BF$_4^-$** and the side chains of **1b**

No. of C-H···O interaction	H···O / Å C-H···O angles	No. of C-H···O interaction	H···O / Å C-H···O angles
A	2.66 (164.2°)	A‘	2.66 (164.2°)
B	2.90 (126.6°)	B‘	2.90 (126.6°)
C	2.52 (168.3°)	C‘	2.52 (168.3°)

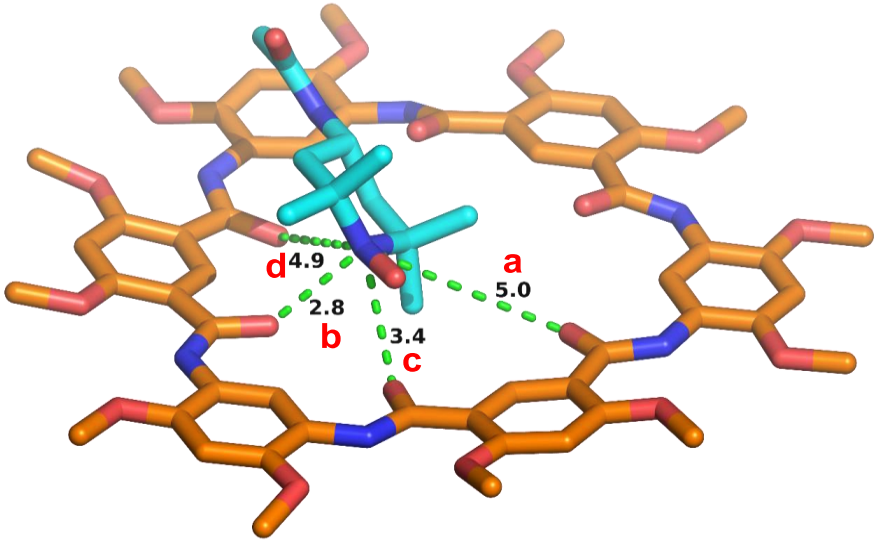

Figure S37 Cation-dipole interactions between **1b** and **AcNH-TEMPO$^+$BF$_4^-$**. The side chains and all hydrogen atoms were omitted for clarity (C orange and cyan, O red, N blue, H white).

Table S7 N$^+$···O cation dipole interactions in the crystal structure of **AcNH-TEMPO$^+$BF$_4^-$⊂1b**

No. of N$^+$···O interaction	O···N$^+$ / Å	No. of O···N$^+$ interaction	O···N$^+$ / Å
a	4.98	c	2.83
b	3.40	d	4.92

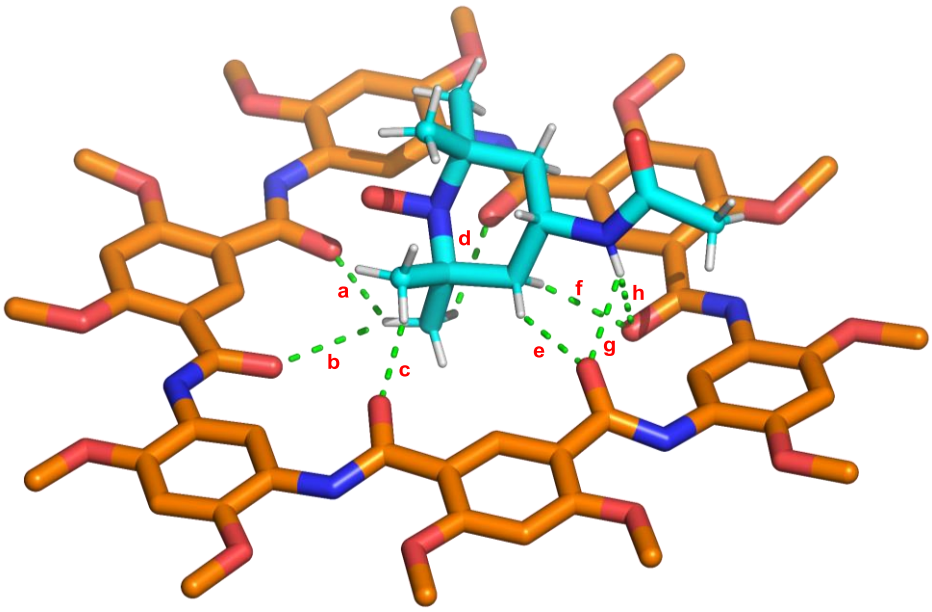

Figure S38 H-bonding interactions between **1b** and **AcNH-TEMPO$^+$BF$_4^-$.** The side chains and part hydrogen atoms were omitted for clarity (C orange and cyan, O red, N blue, H white).

Table S8 H-bonding interactions between **1b** and **AcNH-TEMPO$^+$BF$_4^-$**.

No. of C/N-H···O interaction	H···O / Å C/N-H···O angles	No. of C/N-H···O interaction	H···O / Å C/N-H···O angles
a	2.68 (125.4°)	e	2.38 (146.5°)
b	3.02 (134.2°)	f	2.37 (143.8°)
c	2.38 (158.6°)	g	2.47 (126.0°)
d	2.67 (139.4°)	h	2.82 (127.9°)

DFT calculation for Mulliken charge distribution

All side chains of **CA[6]** are replaced by CH_3 for simplicity. The geometries of **AcNH-TEMPO$^+$**, **AcNH-TEMPO$^+$⊂1c** and **1c** were fully optimized at the B3LYP(PCM,chloroform)/ 6-311G (2d,2p) level of theory with the keyword UAHF method. The contained structures were confirmed without any imaginary frequency. The Mulliken population analysis on these geometries was carried out at the same level. All calculations were performed in Gaussian 09 program package. [5]

(a)

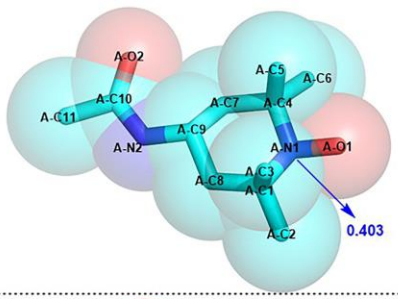

Atom	Mulliken charge	Atom	Mulliken charge
A-N1	0.403	A-N2	-0.121
A-O1	-0.183	A-O2	-0.529
A-C1	0.398	A-C7	-0.543
A-C2	-0.529	A-C8	-0.668
A-C3	-0.549	A-C9	-0.152
A-C4	0.547	A-C10	0.498
A-C5	-0.638	A-C11	-0.570
A-C6	-0.548		

(b)

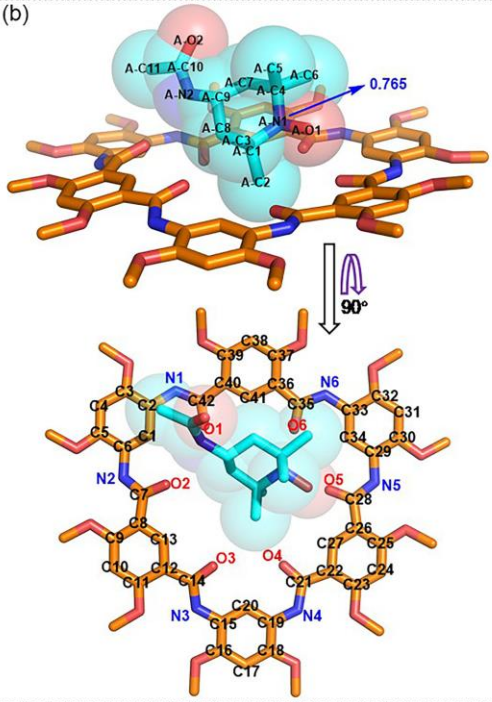

Atom	Mulliken charge	Atom	Mulliken charge
A-N1	0.765	A-N2	-0.355
A-O1	-0.168	A-O2	-0.524
A-C1	-0.349	A-C7	-0.471
A-C2	-0.925	A-C8	-0.695
A-C3	-0.853	A-C9	0.204
A-C4	0.039	A-C10	0.466
A-C5	-0.715	A-C11	-0.670
A-C6	-0.764		

Atom	Mulliken charge	Atom	Mulliken charge	Atom	Mulliken charge
O1	-0.589	C7	0.310	C25	0.381
O2	-0.656	C8	-0.077	C26	-0.266
O3	-0.748	C9	0.336	C27	-0.132
O4	-0.612	C10	-0.311	C28	0.464
O5	-0.603	C11	0.336	C29	0.176
O6	-0.700	C12	-0.165	C30	0.136
N1	-0.390	C13	-0.015	C31	0.155
N2	-0.340	C14	0.475	C32	0.196
N3	-0.415	C15	0.065	C33	0.235
N4	-0.456	C16	0.198	C34	-0.299
N5	-0.430	C17	0.161	C35	0.350
N6	-0.403	C18	0.135	C36	-0.156
C1	-0.206	C19	0.117	C37	0.340
C2	0.191	C20	-0.144	C38	-0.270
C3	0.053	C21	0.313	C39	0.447
C4	0.096	C22	-0.167	C40	-0.377
C5	0.149	C23	0.418	C41	-0.081
C6	0.193	C24	-0.245	C42	0.550

(c)

Atom	Mulliken charge	Atom	Mulliken charge	Atom	Mulliken charge
O1	-0.663	C7	0.414	C25	0.174
O2	-0.630	C8	0.151	C26	0.143
O3	-0.607	C9	0.079	C27	-0.042
O4	-0.583	C10	-0.589	C28	0.494
O5	-0.604	C11	0.241	C29	0.208
O6	-0.611	C12	0.173	C30	0.151
N1	-0.476	C13	-0.090	C31	0.082
N2	-0.509	C14	0.514	C32	0.151
N3	-0.451	C15	0.212	C33	0.142
N4	-0.346	C16	0.149	C34	-0.129
N5	-0.482	C17	-0.072	C35	0.438
N6	-0.454	C18	0.198	C36	0.086
C1	-0.246	C19	0.188	C37	0.158
C2	0.225	C20	-0.091	C38	-0.512
C3	0.085	C21	0.369	C39	0.142
C4	-0.111	C22	0.177	C40	0.126
C5	0.129	C23	0.043	C41	-0.100
C6	0.426	C24	-0.543	C42	0.504

Figure S39 The partial atomic Mulliken charges of all atoms in (a) **AcNH-TEMPO⁺**, (b) **AcNH-TEMPO⁺⊂1c** and **1c** were calculated by Mulliken population analysis. Hydrogen atoms were omitted for clarity.

Standard orientation for the optimized structure of **AcNH-TEMPO⁺**

Center Number	Atomic Number	Atomic Type	Coordinates (Angstroms) X	Y	Z
1	8	0	-3.265253	1.198250	0.445399
2	8	0	3.218756	0.480965	-0.154086
3	7	0	1.882868	0.138846	-0.516534
4	7	0	-2.238374	-0.744413	-0.083651
5	1	0	-2.356601	-1.539715	-0.386729
6	6	0	-0.433592	0.929478	-0.456634

7	1	0	-1.022877	1.652602	-0.193896
8	1	0	-0.519842	0.812384	-1.416330
9	6	0	1.004483	1.323754	-0.138421
10	6	0	-0.881521	-0.337381	0.229536
11	1	0	-0.787709	-0.233125	1.198940
12	6	0	-3.322580	0.032444	0.067117
13	6	0	2.330137	-2.244971	-0.846949
14	1	0	2.202721	-2.030315	-1.773520
15	1	0	2.028528	-3.140781	-0.680811
16	1	0	3.261656	-2.174343	-0.626554
17	6	0	1.527326	-1.269118	0.016818
18	6	0	0.031338	-1.468824	-0.250084
19	1	0	-0.096393	-1.581912	-1.205283
20	1	0	-0.248955	-2.292016	0.179872
21	6	0	1.896383	-1.414625	1.479474
22	1	0	2.816224	-1.168274	1.603816
23	1	0	1.769670	-2.325869	1.753089
24	1	0	1.337634	-0.840839	2.009267
25	6	0	1.203040	1.689306	1.336022
26	1	0	0.777401	1.031185	1.889664
27	1	0	0.814428	2.551089	1.507523
28	1	0	2.141695	1.717368	1.535454
29	6	0	1.448298	2.494350	-0.992323
30	1	0	2.357098	2.719569	-0.780837
31	1	0	0.882642	3.250699	-0.819698
32	1	0	1.386294	2.254796	-1.920668
33	6	0	-4.652398	-0.648715	-0.272879
34	1	0	-5.347821	-0.284787	0.279162
35	1	0	-4.578018	-1.592382	-0.114899
36	1	0	-4.862744	-0.494269	-1.196845

Standard orientation for the optimized structure of **AcNH-TEMPO$^+$⊂1c**

Center Number	Atomic Number	Atomic Type	Coordinates (Angstroms) X	Y	Z
1	8	0	1.261516	7.855115	-0.137480
2	8	0	-6.330367	-5.895025	-0.489015
3	8	0	5.503181	5.559371	-0.314088
4	8	0	-7.582144	-2.393579	-0.123230
5	8	0	-2.365909	8.516789	-0.321531
6	8	0	-3.475191	-2.054156	-0.863091
7	8	0	8.010415	2.861845	-0.597802
8	8	0	3.499016	2.023834	0.448202
9	8	0	-7.640709	2.436183	0.110380
10	8	0	-2.017922	-8.183624	-0.469349
11	8	0	8.118026	-1.993639	-0.964009
12	8	0	5.689382	-4.785198	-0.468892
13	8	0	3.380907	-1.443261	-1.371931
14	8	0	1.574499	-7.303917	-0.272373
15	8	0	-0.377607	-3.627527	-0.666000
16	8	0	-6.546695	5.994989	-0.303912
17	8	0	-3.523115	2.277010	-0.542923
18	7	0	-0.973438	6.269967	-0.142867
19	1	0	-0.623063	7.038462	-0.305160
20	7	0	-5.117728	-3.564622	-0.584084
21	1	0	-5.967050	-3.682642	-0.517355
22	7	0	-5.215185	3.723955	-0.185815
23	1	0	-6.060919	3.789343	-0.044985

24	8	0	-0.520923	4.130263	0.435146
25	7	0	5.370959	2.821499	-0.538608
26	1	0	5.769624	3.530264	-0.818255
27	7	0	5.492113	-2.096914	-0.928054
28	1	0	6.004311	-2.779876	-0.825041
29	7	0	-0.755882	-5.862693	-0.634954
30	1	0	-0.378415	-6.635308	-0.634653
31	6	0	-5.639005	1.290879	-0.324557
32	6	0	-2.922265	-4.702390	-0.640032
33	1	0	-2.485722	-3.883408	-0.698268
34	6	0	2.021323	6.724335	-0.120896
35	6	0	-5.616435	-1.157691	-0.490409
36	6	0	-3.081148	4.972863	-0.159009
37	1	0	-2.600390	4.179307	-0.096308
38	6	0	-2.399218	6.183209	-0.192877
39	6	0	1.907436	9.141087	-0.237035
40	1	0	2.406771	9.217340	-1.180301
41	1	0	2.621014	9.243963	0.553613
42	6	0	1.347697	5.485792	0.050008
43	6	0	-4.690909	-2.299877	-0.661132
44	6	0	-4.313930	-4.727148	-0.601024
45	6	0	-0.122412	5.252582	0.137784
46	6	0	-4.713719	2.480831	-0.357465
47	6	0	4.140330	5.579103	-0.207799
48	6	0	2.120730	4.344592	0.081551
49	1	0	1.685765	3.530575	0.197345
50	6	0	3.403684	6.747839	-0.246875
51	1	0	3.840145	7.561373	-0.358015
52	6	0	-4.226405	-7.138969	-0.499473
53	1	0	-4.663645	-7.958811	-0.458705
54	6	0	-4.471862	4.927638	-0.217941
55	6	0	-6.997492	-1.173751	-0.219804
56	6	0	-5.000824	0.093196	-0.524876
57	1	0	-4.087088	0.117191	-0.696675
58	6	0	-7.025262	1.250829	-0.090107
59	6	0	-2.840845	-7.094742	-0.519898
60	6	0	3.505787	4.325872	-0.048310
61	6	0	-2.176695	-5.855278	-0.593653
62	6	0	-4.961205	-5.965919	-0.539972
63	6	0	6.110132	-0.812462	-0.911122
64	6	0	2.276544	-6.162893	-0.482208
65	6	0	-3.119060	7.363064	-0.274532
66	6	0	7.462604	1.620254	-0.683077
67	6	0	-5.180705	6.125845	-0.269532
68	6	0	4.173762	-2.336139	-1.092326
69	6	0	0.067146	-4.794734	-0.675463
70	6	0	6.059115	1.597904	-0.670353
71	6	0	-7.692929	0.024690	-0.057780
72	1	0	-8.613467	0.006762	0.074772
73	6	0	8.179567	0.436372	-0.801370
74	1	0	9.109257	0.452635	-0.817204
75	6	0	4.343511	-4.908772	-0.593050
76	6	0	3.645830	-3.732253	-0.881616
77	6	0	5.403344	0.381714	-0.828673
78	1	0	4.474876	0.366986	-0.880747
79	6	0	7.500121	-0.772799	-0.896948
80	6	0	6.223497	6.801862	-0.326584
81	1	0	5.835283	7.446855	0.433794
82	1	0	6.111390	7.269527	-1.282419
83	6	0	4.133399	2.973086	-0.006633
84	6	0	2.269972	-3.820441	-0.934039
85	1	0	1.793332	-3.046950	-1.131791

86	6	0	1.543481	-4.993629	-0.709050
87	6	0	3.670117	-6.112996	-0.431367
88	1	0	4.153396	-6.894681	-0.289238
89	6	0	-7.045748	-7.113430	-0.716679
90	1	0	-7.988267	-6.931769	-0.738236
91	1	0	-6.856093	-7.732816	-0.007398
92	1	0	-6.773297	-7.493238	-1.554449
93	6	0	-4.507506	7.338244	-0.313988
94	1	0	-4.985658	8.134027	-0.371068
95	6	0	9.451155	2.946496	-0.613302
96	1	0	9.718335	3.866210	-0.545709
97	1	0	9.784905	2.575577	-1.432996
98	1	0	9.808449	2.454463	0.129796
99	6	0	-8.962307	-2.481604	0.308577
100	1	0	-9.608393	-2.253531	-0.513283
101	1	0	-9.133289	-1.783354	1.101113
102	6	0	-3.088453	9.762174	-0.387532
103	1	0	-2.470398	10.484038	-0.523286
104	1	0	-3.565000	9.899478	0.434670
105	1	0	-3.711473	9.732553	-1.117163
106	6	0	-2.655714	-9.463666	-0.390681
107	1	0	-3.257442	-9.475819	0.358131
108	1	0	-1.991404	-10.146723	-0.278221
109	1	0	-3.148689	-9.625873	-1.198575
110	6	0	9.553645	-1.994659	-0.952803
111	1	0	9.880072	-1.536055	-1.730568
112	1	0	9.873049	-2.900020	-0.957851
113	1	0	9.868139	-1.548904	-0.162920
114	6	0	6.481690	-5.877793	0.048272
115	1	0	6.714439	-6.556536	-0.745476
116	1	0	5.928622	-6.391805	0.806433
117	6	0	-9.076134	2.481117	0.268522
118	1	0	-9.362371	1.873656	1.101564
119	1	0	-9.544559	2.111868	-0.619810
120	6	0	-7.311650	7.189186	-0.297852
121	1	0	-7.038521	7.746350	-1.031588
122	1	0	-7.169265	7.656010	0.527985
123	1	0	-8.241893	6.973634	-0.389399
124	6	0	2.311269	-8.540506	-0.051159
125	1	0	3.159852	-8.343802	0.570221
126	1	0	2.640445	-8.932516	-0.990772
127	8	0	3.749769	-1.529100	3.954998
128	8	0	-2.240391	-1.497148	1.302979
129	7	0	-0.819989	-1.539082	1.185883
130	7	0	3.247740	-0.627599	1.944134
131	1	0	3.576375	-0.323000	1.210951
132	6	0	1.240215	-2.021845	2.417617
133	1	0	1.614566	-2.308388	3.264346
134	1	0	1.519814	-2.658825	1.740675
135	6	0	-0.281103	-2.047656	2.516104
136	6	0	1.802958	-0.665663	2.070499
137	1	0	1.516914	-0.012887	2.742420
138	6	0	4.107950	-1.033425	2.891278
139	6	0	-0.710930	-0.195371	-0.857241
140	1	0	-0.464487	-1.028931	-1.263799
141	1	0	-0.270066	0.525870	-1.311659
142	1	0	-1.661728	-0.078227	-0.916824
143	6	0	-0.290232	-0.202651	0.614442
144	6	0	1.238405	-0.268379	0.704132
145	1	0	1.556325	-0.904681	0.044164
146	1	0	1.596572	0.601000	0.465452
147	6	0	-0.879875	0.984237	1.349532

148	1	0	-1.837509	0.912613	1.357482
149	1	0	-0.623659	1.795858	0.905785
150	1	0	-0.552978	0.996279	2.252364
151	6	0	-0.811647	-1.192842	3.671462
152	1	0	-0.369085	-0.341405	3.669906
153	1	0	-0.641984	-1.639838	4.504836
154	1	0	-1.756964	-1.062927	3.565954
155	6	0	-0.790264	-3.464614	2.687573
156	1	0	-1.748719	-3.457211	2.739306
157	1	0	-0.429112	-3.840458	3.493885
158	1	0	-0.514993	-3.996557	1.936361
159	6	0	5.586747	-0.832504	2.543743
160	1	0	6.083489	-0.663926	3.347257
161	1	0	5.676726	-0.085411	1.948131
162	1	0	5.924691	-1.623969	2.118080
163	1	0	7.260454	6.614859	-0.140435
164	1	0	1.173643	9.915840	-0.158263
165	1	0	-9.384522	3.491103	0.440928
166	1	0	-9.164539	-3.472935	0.656808
167	1	0	1.674829	-9.253746	0.429603
168	1	0	7.388568	-5.493905	0.466725

Standard orientation for the optimized structure of **1c**

Center Number	Atomic Number	Atomic Type	Coordinates (Angstroms) X	Y	Z
1	8	0	4.768309	6.142040	0.112401
2	8	0	-8.247965	-2.653436	-0.094572
3	8	0	7.500806	2.163772	0.098718
4	8	0	-7.771883	1.044186	0.154035
5	8	0	1.842535	8.374712	-0.179017
6	8	0	-3.952875	-0.546333	-0.490244
7	8	0	8.507529	-1.386717	-0.055872
8	8	0	4.097957	-0.045797	0.896343
9	8	0	-5.627174	5.376829	0.268181
10	8	0	-5.451423	-6.651026	0.089507
11	8	0	6.396267	-5.768961	-0.300671
12	8	0	2.957372	-7.132220	0.201105
13	8	0	2.434476	-3.138027	-0.841047
14	8	0	-1.855008	-7.495594	0.355351
15	8	0	-1.914109	-3.348941	-0.176890
16	8	0	-3.027892	8.032635	-0.205145
17	8	0	-2.026734	3.340617	-0.277160
18	7	0	2.056902	5.747719	0.089421
19	1	0	2.720621	6.266889	-0.082702
20	7	0	-6.106110	-1.134211	-0.215911
21	1	0	-6.916689	-0.850718	-0.167728
22	7	0	-2.878134	5.409812	0.001818
23	1	0	-3.602833	5.857357	0.119672
24	8	0	1.478773	3.656845	0.730681
25	7	0	6.138806	-0.220111	-0.062189
26	1	0	6.819639	0.220043	-0.348920
27	7	0	4.011205	-4.665290	-0.328336
28	1	0	4.154983	-5.502645	-0.195826
29	7	0	-3.269107	-5.165042	-0.100850
30	1	0	-3.284935	-6.024311	-0.072193
31	6	0	-4.361885	3.432661	-0.088143
32	6	0	-4.669188	-3.147225	-0.188784

33	1	0	-3.906946	-2.618864	-0.255975
34	6	0	4.929551	4.790656	0.175697
35	6	0	-5.455002	1.237784	-0.193580
36	6	0	-0.409932	5.551509	0.051868
37	1	0	-0.344052	4.628692	0.145998
38	6	0	0.748709	6.317360	0.005658
39	6	0	5.930076	6.989394	-0.002207
40	1	0	6.419985	6.798830	-0.934181
41	1	0	6.603221	6.782620	0.803412
42	6	0	3.763912	4.000482	0.359755
43	6	0	-5.149310	-0.205344	-0.313024
44	6	0	-5.919784	-2.534970	-0.184236
45	6	0	2.348003	4.464524	0.416151
46	6	0	-2.995903	4.069705	-0.126767
47	6	0	6.295362	2.804748	0.170145
48	6	0	3.932014	2.634305	0.438588
49	1	0	3.172787	2.111555	0.563220
50	6	0	6.172277	4.178630	0.084028
51	1	0	6.932563	4.700424	-0.035904
52	6	0	-6.941366	-4.717813	-0.021696
53	1	0	-7.704422	-5.247202	0.028042
54	6	0	-1.667894	6.141867	-0.040941
55	6	0	-6.694812	1.860641	0.042477
56	6	0	-4.336930	2.069859	-0.243046
57	1	0	-3.510639	1.669902	-0.392318
58	6	0	-5.616840	4.035334	0.112236
59	6	0	-5.687549	-5.309348	-0.008300
60	6	0	5.157954	1.983347	0.344138
61	6	0	-4.531024	-4.510820	-0.095530
62	6	0	-7.060827	-3.340979	-0.109294
63	6	0	5.146125	-3.802732	-0.327194
64	6	0	-0.708039	-6.806425	0.135480
65	6	0	0.646128	7.692081	-0.122860
66	6	0	7.455401	-2.245333	-0.124593
67	6	0	-1.752666	7.528915	-0.139585
68	6	0	2.730505	-4.283992	-0.519865
69	6	0	-2.049626	-4.590307	-0.146669
70	6	0	6.195673	-1.626429	-0.146670
71	6	0	-6.769959	3.248889	0.157649
72	1	0	-7.599098	3.656037	0.267379
73	6	0	7.555846	-3.628964	-0.195875
74	1	0	8.391054	-4.037883	-0.188687
75	6	0	1.704387	-6.634150	0.046150
76	6	0	1.622356	-5.279345	-0.288512
77	6	0	5.059831	-2.415757	-0.291730
78	1	0	4.227178	-2.008282	-0.366790
79	6	0	6.401415	-4.399195	-0.278998
80	6	0	8.708017	2.941480	0.074050
81	1	0	8.647555	3.717306	0.808448
82	1	0	8.832004	3.376949	-0.895431
83	6	0	5.100129	0.495349	0.434600
84	6	0	0.357980	-4.733763	-0.373394
85	1	0	0.288155	-3.835159	-0.601899
86	6	0	-0.825570	-5.439934	-0.138210
87	6	0	0.554687	-7.394194	0.220162
88	1	0	0.627320	-8.304956	0.393445
89	6	0	-9.437097	-3.419924	-0.310379
90	1	0	-10.193167	-2.830269	-0.360087
91	1	0	-9.558355	-4.033872	0.418354
92	1	0	-9.358047	-3.909662	-1.131507
93	6	0	-0.600742	8.300213	-0.196645
94	1	0	-0.663353	9.224013	-0.285147

95	6	0	9.828821	-1.967212	-0.037152
96	1	0	10.484744	-1.267994	0.014686
97	1	0	9.966283	-2.476321	-0.838888
98	1	0	9.914412	-2.542950	0.726491
99	6	0	-9.045493	1.607941	0.552973
100	1	0	-9.507488	2.077509	-0.290215
101	1	0	-8.888682	2.333423	1.323679
102	6	0	1.767214	9.809500	-0.293558
103	1	0	2.647689	10.166298	-0.431280
104	1	0	1.396215	10.175737	0.512790
105	1	0	1.207356	10.042303	-1.037704
106	6	0	-6.603019	-7.497493	0.183300
107	1	0	-7.152689	-7.209763	0.916798
108	1	0	-6.323979	-8.403807	0.329084
109	1	0	-7.106604	-7.444433	-0.632552
110	6	0	7.673684	-6.422483	-0.253300
111	1	0	8.181919	-6.188635	-1.033557
112	1	0	7.545775	-7.373658	-0.228211
113	1	0	8.147715	-6.142615	0.533140
114	6	0	3.159276	-8.447791	0.764559
115	1	0	3.066348	-9.184047	-0.006279
116	1	0	2.424270	-8.628514	1.520870
117	6	0	-6.886334	6.074965	0.388986
118	1	0	-7.427207	5.692195	1.229131
119	1	0	-7.461443	5.929931	-0.501584
120	6	0	-3.165094	9.443550	-0.247488
121	1	0	-2.659918	9.790816	-0.987490
122	1	0	-2.835088	9.821645	0.570036
123	1	0	-4.090336	9.671799	-0.357142
124	6	0	-1.764773	-8.923873	0.625152
125	1	0	-0.926801	-9.114169	1.262717
126	1	0	-1.639631	-9.453651	-0.296030
127	1	0	9.543863	2.309578	0.290757
128	1	0	5.628777	8.015264	0.039136
129	1	0	-6.702865	7.119794	0.528878
130	1	0	-9.680916	0.829246	0.920086
131	1	0	-2.661589	-9.253184	1.106997
132	1	0	4.136682	-8.504752	1.196222

---

^{1}H NMR Spectra

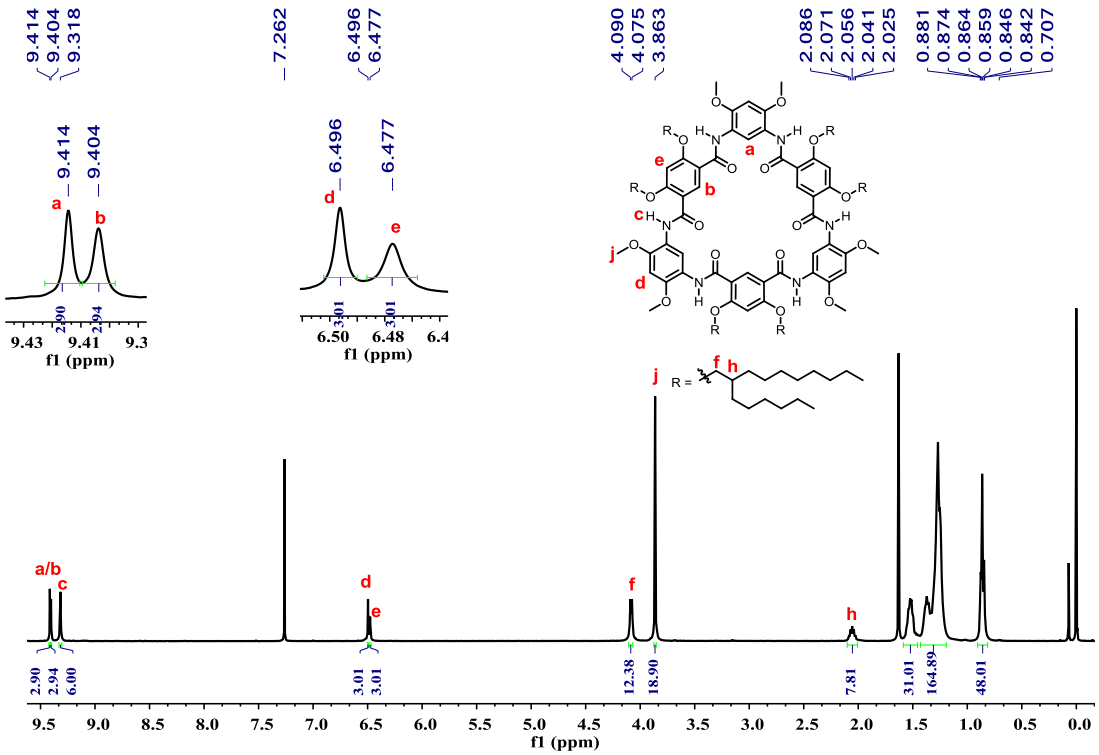

^{1}H NMR spectrum ($CDCl_3$, 400 MHz, 298 K) of **1a**.

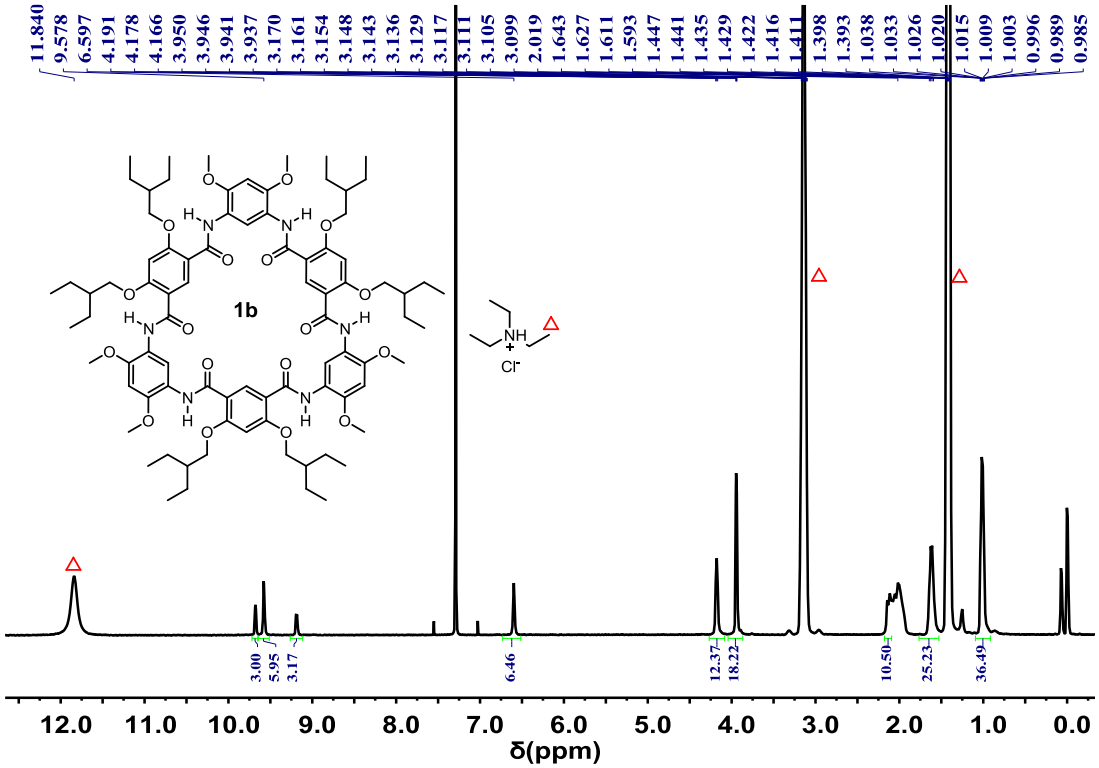

^{1}H NMR spectrum ($CDCl_3$, 400 MHz, 298 K) of **1b** in the presence of **Et_3N·HCl** (Δ).

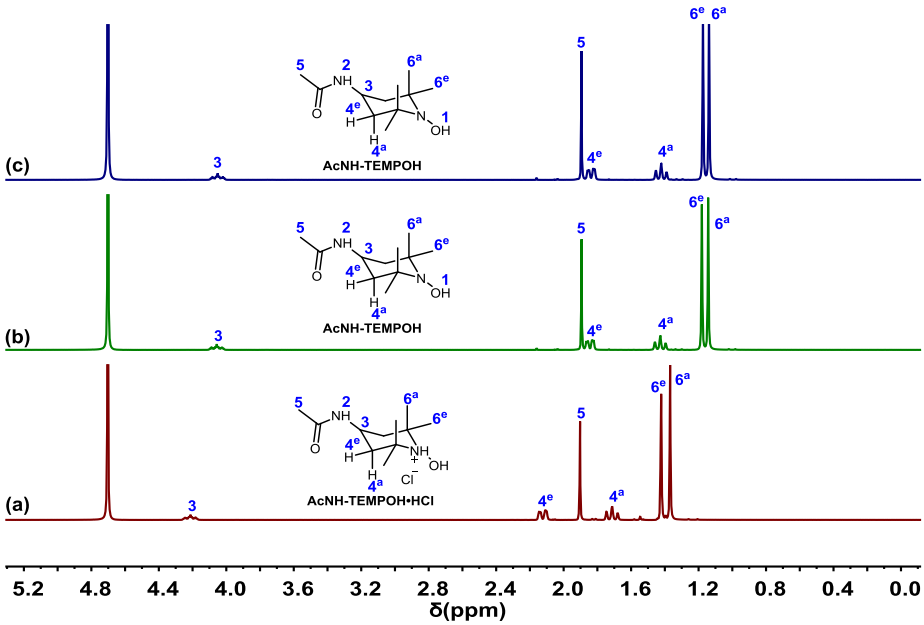

^{1}H NMR spectra (400 MHz, D_2O, 298 K) of (a) **AcNH-TEMPOH·HCl**; (b) after adding excess $NaHCO_3$ to the above solution; (c) **AcNH-TEMPOH·HCl** in the presence of excess $NaHCO_3$.

References

[1] a) L. H. Yuan, W. Feng, K. Yamato, A. R. Sanford, D. G. Xu, H. Guo, B. Gong, *J. Am. Chem. Soc.* **2004**, 126, 11120-11121; b) Y. A. Yang, W. Feng, J. C. Hu, S. L. Zou, R. Z. Gao, K. Yamato, M. Kline, Z. H. Cai, Y. Gao, Y. B. Wang, Y. B. Li, Y. L. Yang, L. H. Yuan, X. C. Zeng, B. Gong, *J. Am. Chem. Soc.* **2011**, 133, 18590-18593; c) J. C. Hu, L. Chen, Y. Ren, P. C. Deng, X. W. Li, Y. J. Wang, Y. M. Jia, J. Luo, X. S. Yang, W. Feng, L. H. Yuan, *Org. Lett.* **2013**, 15, 4670-4673; d) L. Q. Yang, L. J. Zhong, K. Yamato, X. H. Zhang, W. Feng, P. C. Deng, L. H. Yuan, X. C. Zeng, B. Gong, *New J. Chem.* **2009**, 33, 729-733; e) X. W. Li, B. Li, L. Chen, J. C. Hu, C. D. Y. Wen, Q. D. Zheng, L. X. Wu, H. Q. Zeng, B. Gong, L. H. Yuan, *Angew. Chem. Int. Ed.*, **2015**, 54, 11147-11152.

[2] V. D. Sen, I. V. Tikhonov, L. I. Borodin, E. M. Pliss, V. A. Syroeshkin, A. I. Rusakov, *J. Phys. Org. Chem.* **2015**, 28, 17-24

[3] Gabriel Tojo, Marcos Fernández. *Oxidation of Alcohols to Aldehydes and Ketones.* Springer US, **2006**, P243.

[4] J. M. Bobbitt, N. A. Eddy, C. X. Cady, J. Jin, J. A. Gascon, S. Gelpí-Dominguez, J. Zakrzewski, M. D. Morton, *J. Org. Chem.* **2017**, 82, 9279-9290.

[5] Gaussian 09, Revision E.01, M. J. Frisch, G. W. Trucks, H. B. Schlegel, G. E. Scuseria, M. A. Robb, J. R. Cheeseman, G. Scalmani, V. Barone, B. Mennucci, G. A. Petersson, H. Nakatsuji, M. Caricato, X. Li, H. P. Hratchian, A. F. Izmaylov, J. Bloino, G. Zheng, J. L. Sonnenberg, M. Hada, M. Ehara, K. Toyota, R. Fukuda, J. Hasegawa, M. Ishida, T. Nakajima, Y. Honda, O. Kitao, H. Nakai, T. Vreven, J. A. Montgomery, Jr., J. E. Peralta, F. Ogliaro, M. Bearpark, J. J. Heyd, E. Brothers, K. N. Kudin, V. N. Staroverov, T. Keith, R. Kobayashi, J. Normand, K. Raghavachari, A. Rendell, J. C. Burant, S. S. Iyengar, J. Tomasi, M. Cossi, N. Rega, J. M. Millam, M. Klene, J. E. Knox, J. B. Cross, V. Bakken, C. Adamo, J. Jaramillo, R. Gomperts, R. E. Stratmann, O. Yazyev, A. J. Austin, R. Cammi, C. Pomelli, J. W. Ochterski, R. L. Martin, K. Morokuma, V. G. Zakrzewski, G. A. Voth, P. Salvador, J. J. annenberg, S. Dapprich, A. D. Daniels, O. Farkas, J. B. Foresman, J. V. Ortiz, J. Cioslowski, and D. J. Fox, Gaussian, Inc., Wallingford CT, **2013**.